UNIVERSITY OF CALIFORNIA,
IRVINE

Investigation of LiDAR for Traffic Monitoring with Emphasis on Heavy Duty Trucks

DISSERTATION

submitted in partial satisfaction of the requirements
for the degree of

DOCTOR OF PHILOSOPHY

in Civil Engineering

by

Koti Reddy Allu

Dissertation Committee:
Professor Stephen G. Ritchie
Professor R. Jayakrishnan
Assistant Professor Michael F. Hyland

2024

DEDICATION

To

my parents, brothers, sisters, and friends

my dissertation committee,
faculty and staff at Institute of Transportation Studies

in recognition of their support and guidance

TABLE OF CONTENTS

LIST OF FIGURES

LIST OF TABLES

ACKNOWLEDGEMENTS

I would like to express the deepest appreciation to my committee chair, Professor Stephen G. Ritchie for his invaluable support throughout my PhD journey, who instilled a spirit of adventure regarding research and scholarship, and an excitement regarding teaching. Without his trust in me, guidance, and infinite patience this dissertation would not have been possible.

I would like to thank my committee members, Professor R. Jayakrishnan and Professor Michael Hyland, whose research, enthusiasm, and excitement towards Transportation Research motivated me to think and reach beyond the horizon both in current times as well as challenging times.

In addition, I would like to thank all the faculty at the Institute of Transportation Studies whose classes have taught all the concepts and research ideas. A heartfelt thanks to Professor Wenlong Jin for his words of wisdom, kindness, and support during challenging times.

I would like to thank all my friends and faculty from previous academic institutions who made me reach here as well as friends I made at UC Irvine who immensely contributed to my intellectual growth and increased my appetite to strive for the betterment of society without worrying about the time and challenges it takes.

Finally, I would like to express sincere gratitude to the undergraduate students in the Department of Civil and Environmental Engineering for making my PhD journey in the department memorable.

VITA

Koti Reddy Allu

2004 - 08	Bachelor of Technology in Civil Engineering, National Institute of Technology, Calicut, India
2011-13	Master of Technology in Civil Engineering - Transportation & Infrastructure Engineering, Indian Institute of Science, Bangalore, India.
2015– 24	PhD in Civil Engineering at University of California, Irvine.
2016-24	Graduate Student Researcher at Institute of Transportation Studies, UCI.
Fall 2016, 17, 19, 23	Teaching Assistant for CEE121- Transportation Systems I – Analysis and Design
Spring 2017, 18	Teaching Assistant, ENGRCEE124 – Transportation Systems IV: Freeway Operations and Control
Fall 2017 – Spring 2018	Mentor to ITE Student Chapter at UC Irvine

FIELD OF STUDY

Transportation Systems Engineering

ABSTRACT OF THE DISSERTATION

Investigation of LiDAR sensor for Traffic Monitoring with Emphasis on Heavy Duty Trucks

by

Koti Reddy Allu

Doctor of Philosophy in Civil Engineering

University of California, Irvine, 2024

Professor. Stephen G. Ritchie, Chair

Traffic Monitoring is at the center of any Intelligent Transport System. Current traffic monitoring sensors are challenged to deliver in the evolving landscape of connected, autonomous and alternative fuel transportation systems. This dissertation explores the feasibility of emerging LiDAR technology for traffic monitoring, in an infrastructure-based, side-fire LiDAR configuration. LiDAR technology was investigated in terms of providing both the core data elements of existing traffic monitoring systems such as vehicle counts and speeds, as well as more high-resolution data elements required for future connected and autonomous vehicles such as relative positions of vehicles on a roadway, vehicle lateral and longitudinal positions within a lane, physical attributes of individual vehicles, and vehicle microscopic trajectories. LiDAR sensors were deployed at both dense urban corridors and rural highway locations. At the urban location, the LiDAR estimate of vehicle counts across lanes was between 87% to 110% of a baseline calibrated sensor's vehicle counts. At the rural highway location, microscopic trajectories for

vehicles were derived at 0.1 second resolution, enabling detection of anomalies in vehicle behavior. In addition, the precise lateral positions of heavy-duty vehicles were derived at the urban corridor location, with a particular interest being future safety assessment for loss of control of autonomous heavy-duty trucks. The high-resolution traffic data elements derived from this research can assist in detecting anomalous behavior of vehicles, whether from impaired driving or loss of effective autonomous control, with road safety assessments, and in providing inputs for microscopic road emission modeling.

1. Introduction

1.1. Background

Transportation Planning and Traffic Management agencies have been striving to provide safe, affordable, efficient, and environmentally friendly options for both people and goods movement with the help of Intelligent Transportation Systems. Traffic monitoring is a process of collecting road user information either using stationary or mobile sensors, and is a key component of any such Intelligent Transportation System (*1*). Recent efforts in the automotive industry, logistics industry, ecommerce, and transport network companies, to accelerate the road trial and adoption of connected, automated and alternative fuel vehicle technologies have added new challenging dimensions to traffic monitoring.

The core functional requirements of a traffic monitoring system include (i) detection of road users, (ii) classification of road users by type (e.g., vehicle, bicycle, or pedestrian), (iii) speed estimation of road users through tracking, and (iv) assessment of road-user interactions for safe maneuvering guidance. Currently these functionalities are fulfilled partly or fully by existing sensors such as Inductive Loop Detectors (ILD), Video Cameras, Piezoelectric Sensors, Bluetooth or Wi-Fi Mac ID readers, Radars, Magnetometers, etc. (*2*).

Figure 1.1. Inductive Loop Detectors and Video Cameras on I-405/Sand Canyon Drive

Bernas et al. (*2*) outline a number of low-cost vehicle detection sensing technologies like wireless network signal strength assessment, accelerometers, magnetometers, radars, and acoustic sensors, but only ILD and video camera-based traffic monitoring are used heavily in current practice. All the sensing technologies mentioned have limitations either in terms of detection rates or granularity of the data being collected. For example, ILDs (6ft wide) have been used for vehicle detection, speed estimation and even vehicle type classification (*3*, *4*) within their detection range. ILDs have a detection range of 6 ft plus the length of vehicles passing through; hence, for traffic monitoring, current practice requires one ILD per lane. Also, prior research outlines the limitations of video cameras under different lighting conditions as well as weather conditions(*5*). The strengths and weaknesses of the two most widely used detectors, namely ILD and video cameras, from the Traffic Control Systems Handbook (*6*) are presented in Table 1.1 below.

Table 1.1. Strengths and Weaknesses of ILD and Video Camera

Technology	Strengths	Weaknesses
Inductive Loop	Flexible design to satisfy large variety of applications.	Installation requires pavement cut.
	Mature, well-understood technology.	Improper installation decreases pavement life.
	Large experience base.	Installation and maintenance require lane closure.
	Provides basic traffic parameters (e.g., volume, presence, occupancy, speed, headway, and gap).	Wire loops subject to stresses of traffic and temperature.
	Insensitive to inclement weather such as rain, fog, and snow.	Multiple detectors usually required to monitor a location.
	Provides best accuracy for count data as compared with other commonly used techniques.	Detection accuracy may decrease when design requires detection of a large variety of vehicle classes.
	Common standard for obtaining accurate occupancy measurements.	
Video Image Processor	Monitors multiple lanes and multiple detection zones/lane.	Installation and maintenance, including periodic lens cleaning, require lane closure when camera is mounted over roadway (lane closure may not be required when camera is mounted at side of roadway)
	Easy to add and modify detection zones.	Performance affected by inclement weather such as fog, rain, and snow; vehicle shadows; vehicle projection into adjacent lanes; occlusion; day-to-night transition; vehicle / road contrast; and water, salt grime, icicles, and cobwebs on camera lens.
	Rich array of data available.	Requires 50- to 70-ft (15- to 21-m) camera mounting height (in a side-mounting configuration) for optimum presence detection and speed measurement.
	Provides wide-area detection when information gathered at one camera location can be linked to another.	Some models susceptible to camera motion caused by strong winds or vibration of camera mounting structure.
	Generally cost-effective when many detection zones within the camera field-of-view or specialized data are required.	Movement from other structures (i.e. span wires or overhead conductor) within field of view can cause problems.
	High frequency excitation models provide classification data.	

1.2. Traffic Monitoring of Commercial Vehicles

Road freight transportation systems play a vital role in the economy of a region and entails movement of a wide variety of commodities with the help of commercial vehicles. Understanding the seasonal, temporal, and spatial patterns of the class-based commercial vehicle activities through surveillance is important for planning and operating agencies (*3*). Class-based surveillance data is useful in freight forecasting models, air pollution assessment, assessing the health impacts on adjoining communities, and road network asset management (*7*). Various sensing technologies have been used for monitoring commercial vehicle activities. Determining the body type or class of the commercial vehicle and reidentification of the same commercial vehicle in the road network have been two important research problems associated with monitoring the commercial vehicle activities. Moreover, the commercial vehicle classification problem is closely associated with understanding which types of commodities are carried (*8*).

Asborno et al., (*9*) synthesized information about the sensing technologies from FHWA's Traffic Detector Handbook. As per their work even though intrusive sensors such as advanced ILD perform quite accurately, the installation and maintenance costs of these sensors as well as the pavement surface quality in high volume freight corridors are deterring factors for this sensor. GPS and Cellphone-based sensors are generally present within commercial vehicles, but data from these sensors is proprietary even if it can be purchased. Won, M (*10*) also provides a state-of-the-art comprehensive review of Intelligent Traffic Monitoring Systems for the vehicle classification.

Most of the sensors mentioned above can classify vehicles based on length, while inductive loops, WIM, microwave radars, active infrared radars, and cameras can be used for axle-based classification. Hernandez, S.V., et al., (*3*) showed that more than 50 body types can be classified using ILD signature data. The performance of ILD is highly dependent on pavement conditions and ILD maintenance is difficult and expensive.

While several sensors are presented from the traffic monitoring perspective, along with their own challenges, none of the sensors can obtain and provide direct three-dimensional geometry of commercial vehicles. Detecting and monitoring the commercial vehicle's geometry on the road is still a relatively unexplored research area, despite commercial vehicle identification and classification providing significant value to transport planning agencies.

Light Detection and Ranging (LiDAR) sensors have been widely adopted as mobile sensors in the development of autonomous vehicles, but their potential for traffic monitoring in an infrastructure-based, fixed-location, side-fire configuration is just emerging. The advantage of LiDAR sensors over most others is that they can perform traffic monitoring in 360 degrees, 24 hours of the day under most weather conditions, for a range of up to 650 ft(*11*). Being in the early stages of adoption, stationary LiDAR data processing algorithms for traffic monitoring are developed on a need basis but efficient universally applicable algorithms are yet to be developed. Most of the algorithms for vehicle classification focus on highway facilities without lane consideration(*7*, *9*, *12–15*).

1.3. Objective

The objective of this dissertation is to develop efficient data processing algorithms for infrastructure-mounted LiDAR sensors on highway facilities that can automatically detect lane boundaries and perform lane-based object detection, derive traffic parameters (e.g., vehicle count, classification, speed etc.) using single LiDAR object scans or aggregated LiDAR object scans, and develop corresponding applications (e.g., anomalous trajectory detection, safety assessment).

One critical data process problem relates to background subtraction. It is the process of identifying and removing stationary objects like roadside buildings, noise barrier walls, etc.. Existing background subtraction algorithms for infrastructure mounted LiDAR sensor are tailor made and require manual parameter tuning based on facility type and traffic conditions. The current dissertation aims to develop a background subtraction algorithm that automatically detects lane boundaries without any manual intervention.

Further, this dissertation proposes establishing virtual LiDAR loops on individual travel lanes, lane-based object detection, and virtual loop actuation-based volume counts.

This dissertation also aims to identify and adopt an efficient multiple object tracking and data association procedure from the computer vision literature for tracking vehicles across LiDAR scans. It then aims to enhance the details of LiDAR scanned vehicles and expand the pool of applications by aggregating the individual LiDAR scans of same vehicle by developing a suitable reconstruction framework.

This dissertation also focuses on the development of a framework for deriving microscopic trajectories of vehicles based on the aggregated LiDAR scans of each vehicle. It aims to identify anomalous microscopic trajectories and develop algorithms for two very important applications. The first one is anomaly detection in the lateral position of autonomous trucks which can help in developing safe remote intervention control strategies. The second application is identification of impaired driving behavior at the LiDAR sensor locations.

1.4. Dissertation Contributions and Outline

This section lists the contributions of this dissertation by chapter and outlines the rest of the dissertation. Chapter Two presents a novel lower bound on the largest radial distance-based static background elimination algorithm which can be employed for a stationary LiDAR sensor installed on any road facility without any need for manual parameter tuning. The proposed background elimination algorithm also enables automatic identification of lane boundaries, and establishment of LiDAR virtual loops in each lane—a unique contribution based on the author's knowledge. This further enables lane-based object detection using DBSCAN clustering and volume counts on a high-density urban freeway corridor. From the field data collected, volume counts from the LIDAR-based system range from 87% on the fast lane to 110% on the slow lane in comparison to Truck Activity Monitoring System (TAMS)(*16*). The dissertation also presents a vehicle length-based identification of medium and heavy-duty vehicles using Gaussian Mixture Models (GMM) clustering.

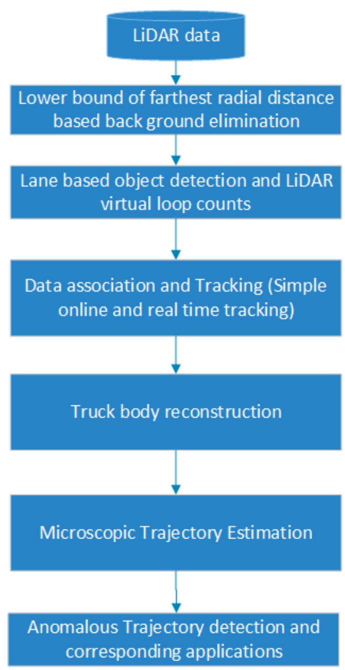

Figure 1.2. Outline of the Dissertation

Chapter Three presents and adopts a simple but efficient combination of Hungarian algorithm for data association and Kalman filter for multiple-object tracking known as Simple Online and Realtime Tracking (SORT) identified from computer vision literature(*17*). This approach maps and groups the individual LiDAR scans of the same vehicle. It further develops and presents a two-stage multiway registration framework for aggregating the LiDAR scans of same vehicle with the aim of recreating the actual geometry of vehicle. This chapter also presents he recreated geometries for nine types of heavy-duty trucks.

Chapter Four develops and tests multiple pairwise registration frameworks to identify optimal pairwise registration of LiDAR vehicle scans. This optimal pairwise registration is applied for aggregating all the LiDAR scans of the same vehicle and recreating its actual geometry. This recreated geometry is invert transformed to the original individual scan position for estimating the microscopic vehicle trajectory. This approach involves two stages and is called forward pass-backward pass trajectory estimation. It distinguishes itself from earlier works in two ways. First, it uses the fully recreated LiDAR-based vehicle for trajectory estimation. Second, it estimates the vehicle trajectory in the backward direction whereas other works estimate trajectories using single scans in the forward direction.

Chapter Five presents two important applications based on identifying anomalous microscopic trajectories. The first one is an illustration of concept to detect anomalies in the lateral lane position of an autonomous heavy-duty vehicle which is important for developing remote control intervention strategies. The second application presented is detection of microscopic trajectories that are likely impaired driving. A new heuristic called “Surrogate Risk Score” is introduced and several futuristic control strategies are discussed.

Chapter Six presents the conclusions and findings of the current dissertation and proposes future research.

2. LiDAR Background Subtraction and Object Detection

An infrastructure-mounted LiDAR sensor captures point clouds of its target environment, which comprises moving vehicles on the road as well as the static objects such as the road infrastructure, buildings, and vegetation, within its detection zone. To derive traffic related information, the LiDAR raw point cloud data must be processed in sequential steps. The first of these data processing steps is to determine the boundary or edge of the travel lanes in case of highways and eliminate the buildings and vegetation for improving computational efficiency of data processing. Once the boundaries are determined, the next step is to separate the static road surface, traffic signs, etc. as background and extract the parts of point cloud that corresponds to vehicles.

2.1. LiDAR Basics

2.1.1. Early days LiDAR applications

Light Detection and Ranging (LiDAR) is an active remote sensing technique used to obtain the three-dimensional information of a target environment. LiDAR sensors emit rapid pulses of laser light and capture the light energy reflected off a target. The time taken between the light energy emission and return capture is used to estimate the distance of the target from the LiDAR sensor. The amount of reflected light energy received by the LiDAR sensor depends on the reflective characteristics of the target surface and is generally referred to as intensity (*18*).

In the late 1980s, airborne LiDAR sensors were used in combination with Global Positioning System(GPS) and Inertial Measurement Unit (IMU) for developing detailed topographic digital elevation models, which further led to development of vegetation and land cover assessment models(*18*). While LiDAR provided the geometry of its scanned environment, GPS continuously recorded the location of airborne LiDAR sensor based on triangulation and IMU provided the orientation of LiDAR sensor with reference to chosen global reference coordinate system. The technology advancements vastly expanded the applications for

LiDAR use such as impact assessment of hazards like landslides, floods, lava flows, city planning, climate monitoring, people and vehicle counting (*19*) to name a few.

2.1.2. LiDAR in Transportation

LiDAR sensors made their way into transportation as part of vehicle mounted arrays of sensors for developing autonomous driving. They further made inroads in the form of infrastructure-mounted sensors to aid in the development of transport applications and smart roadways(*20*). A schematic of infrastructure-mounted LiDAR sensors is presented in Figure 2.1 below.

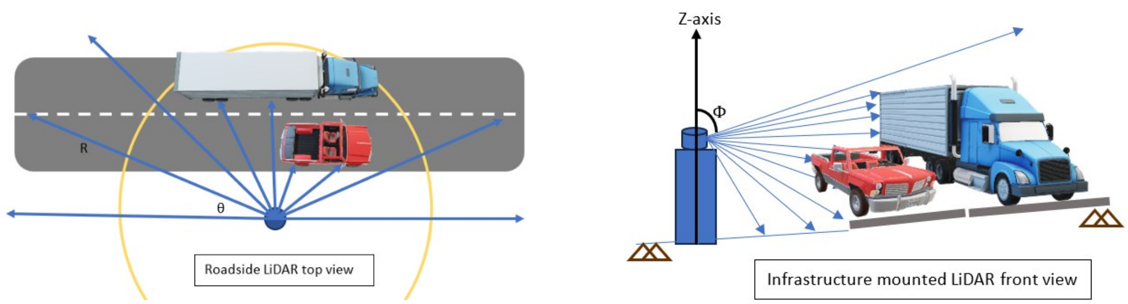

Figure 2.1. Infrastructure-mounted LiDAR Sensor (a) top view (b) side view

The infrastructure-mounted LiDAR sensors emit a vertical array of laser beams (16 or 32) rotating horizontally at a high frequency to capture the surrounding target environment. The scanned environment is provided as a three-dimensional point cloud for further analysis. These scans consist of both the static background such as buildings, trees, sound barrier walls, road surface etc., as well as the vehicles passing through. The current chapter focuses on the first step of identification and removal of the static background from the LiDAR point clouds. After background subtraction, the foreground consists of points clouds of vehicular objects and other road users present in the entire LiDAR detection zone.

2.2. Background Subtraction and Object Detection

2.2.1. Previous work

The three-dimensional scans of a LiDAR sensor are generally provided in spherical coordinates (r, θ, Φ). It comprises the radial distance (r) of a scan point, the azimuthal angle (θ) in the horizontal plane and the polar angle (Φ) in the vertical plane. In general, these scans are converted from spherical coordinates to cartesian coordinates for analyzing and deriving the traffic parameters.

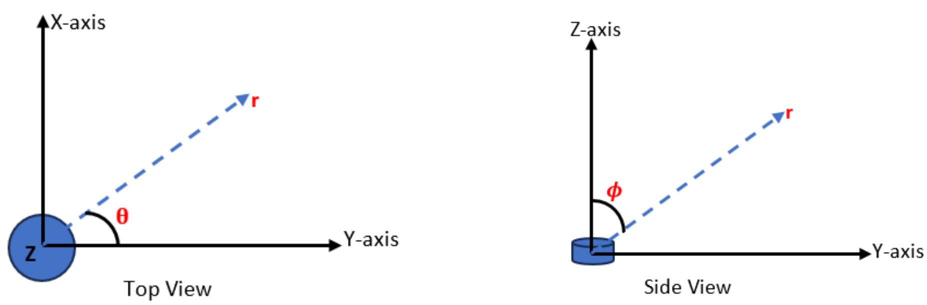

Figure 2.2. Spherical coordinate system of LiDAR sensor

Zhang et al.(*21*) used a height threshold-based background mask to remove the road infrastructure and obtain vehicle points. Sun et al. (*22*) manually selected just the points within road boundaries and removed the road surface points using the RANSAC algorithm. Wu, Jianqing proposed (*23*) a 3D-Desnsity Statistic Filter (3D-DSF) to separate the background points from the vehicular points. 3D-DSF works on the principle that in aggregated observations of LiDAR scans the static background grids will have more density compared to moving vehicle grids. Li, Y et al. (*24*) also used a 3D occupancy based background filtering for obtaining vehicular point clouds. A spatial occupancy-based LiDAR background subtraction algorithm was devised for removal of the static background. The previous works manually selected the region of interest comprising the road boundaries and eliminated other static background such as roadside buildings and trees. Also, the density and occupancy-based background methods require selection of a threshold value for separating static point grids with respect to the moving point grids. A single threshold value will not work in all the traffic scenarios of light, medium and dense traffic. In light traffic conditions, the background point grids will have high occupancy whereas under heavier traffic conditions, the me background point grids will have lower occupancy. To overcome this shortcoming and have a background mask that works under all traffic scenarios, this research proposes a novel lower bound of farthest radial distance-based background mask.

2.2.2. Lower Bound based Farthest Radial distance Background Mask

Two important distinctions of the background mask proposed here compared to the ones mentioned in the previous section are, (1) the entire scans of the LiDAR are used without manually removing the buildings or trees or other static objects and (2) no manual threshold selection of any heuristic or parameter is used in estimating the background mask. In this way, the proposed background mask algorithm can be used for LiDAR sensors mounted either on rural highways, dense urban freeway corridors or urban arterials. This is a clear distinction from the previously mentioned background mask estimation procedures.

For developing the background mask, the LiDAR scans were aggregated for a small duration and the aggregated point cloud divided into Polar - Azimuth $(\Phi - \Delta\theta)$ grids from the sensor location to the maximum 650 ft range. Each grid's angular size $\Delta\theta$ was chosen such that at a range of 650 ft, the horizontal resolution of the grid was 1 foot. This horizontal resolution would not be constant throughout the scan range and increases from a minimum at the sensor location to the maximum at the range of 650ft. At this stage the LiDAR scan environment was divided into 32 radial discs, one for each of the LiDAR beams. These discs were further split into 0.82 feet cells in radial direction, creating a mesh-grid of the scan environment. This mesh grid acts as a basis for the estimation of the background mask.

The principle behind this background mask filter is to identify the farthest grid with LiDAR points present in each of the $\Phi - \Delta\theta$ radial wedges of the mesh-grid. Although this heuristic seems logical, it might not be able to accurately eliminate the background if it is not planar in nature, like a tree shrub. To overcome this and be able to even eliminate non-planar background objects, the final contiguous chunk having LiDAR scan points was identified as background. This would be the lower bound of the farthest radial distance after which the LiDAR points were considered static background.

The proposed algorithm was applied for a LiDAR sensor deployed on Northbound Interstate -710 at Willow near the Port of Los Angeles. This is a dense urban corridor with three lanes in each direction and is shown in Figure 2.2. For this site, a 60-second aggregated pointcloud (3) of size ~14.6 million points was used to estimate the background mask. The LiDAR scan environment was converted into a mesh-grid of size 32 x 2179 x 800. The algorithm resulted in a background mask of size 132,384 grid cells.

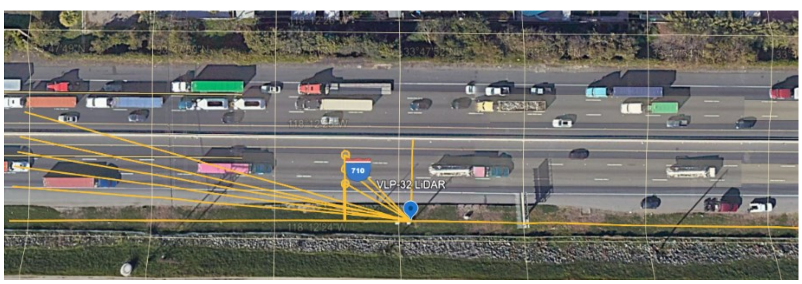

Figure 2.3. LiDAR site at Interstate-710

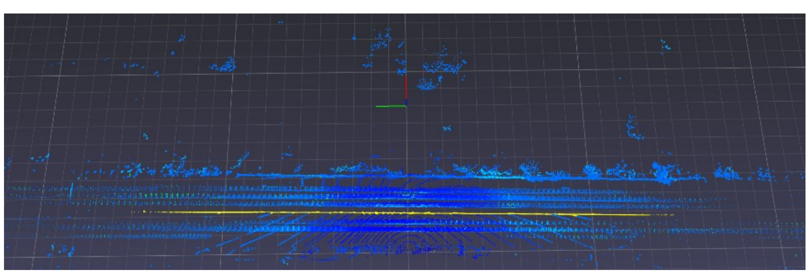

Figure 2.4. Aggregated point clouds for 60-second duration

The algorithm identified 83.6% of points as background and 16.4% of points as vehicular points. The resultant background and foreground are shown in Figure 2.5 and Figure 2.6 . The foreground still consists of some points from the trees in the far background, creepers on the sound barrier wall and the plants on the ground adjacent to the shoulder. All these non-foreground points comprise 16% of the total foreground points and 2.7% of the total aggregated point cloud. This indicates scope for improvement of the proposed lower bound of the far radial distance algorithm.

Aggregation Interval	Frames	Total Points	Estimated Background Points	Estimated Foreground Points	Misidentification
60 seconds	76239 - 76838	14581082	12199021	2378570	392000
Percent		100%	83.66%	16.31%	2.69%

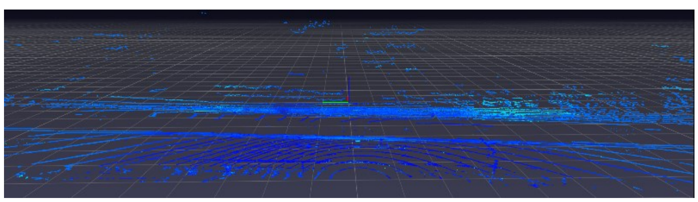

Figure 2.5. Identified Background point at I-710

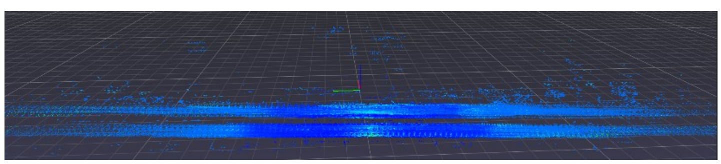

Figure 2.6. Identified Vehicular points at I-710

2.3. Median and Lane Marking identification

The background points identified by the proposed algorithm consisted of the trees in the far background, sound barrier wall on the far side of road and a median separating the roadway in both directions. The point cloud of this static background was further processed using DBSCAN, a density-based clustering algorithm to separate into sound barrier wall, road plane and median.

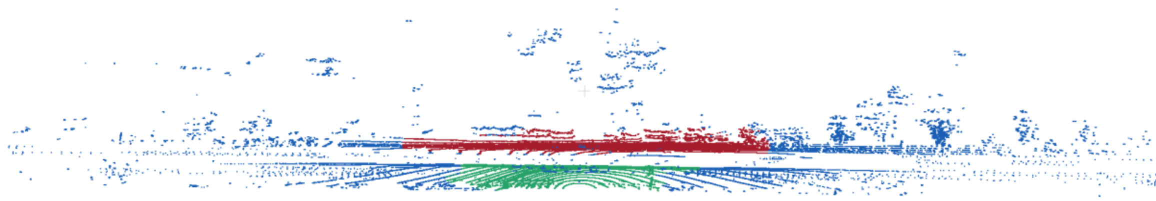

Figure 2.7 DBSCAN clustering (a) Red - Sound Barrier Wall (b) Green - Road Surface and Median (c) Blue - Noise

The point cloud of the road surface and median was further segmented into just the road surface plane and median plane using the Random Sample Consensus (RANSAC) algorithm (Table 2.1). RANSAC is a general parameter estimation algorithm for data with outliers. It uses the minimum number of points to estimate the parameters and then expands upon the data points that comply with the estimated parameters. It is a widely used algorithm for segmentation purposes in point cloud datasets (*25*). From the table, it can be seen that the road plane has a unit normal in the positive z-axis direction whereas the median plane has a unit-normal in the positive x-axis direction. These confirm the LiDAR sensor installation configuration form the field.

Table 2.1. Road and Median Plane Equations at I-710

Plane	x-coefficient	y-coefficient	z-coefficient	constant
Road	-0.06415	-0.02841	0.99754	3.08377
Median	0.99125	-0.01604	-0.13100	-20.50467

The intensity values of the identified road surface points were used to extract the points corresponding to the lane markings. Due to the better reflective characteristics of the lane markings, their corresponding points would have higher intensity values compared to the road surface points. The histogram of intensity values for the road surface points are shown in Figure 2.8 below. Gaussian Mixture Modeling (GMM) of the road surface points based upon intensity values was performed to extract the points corresponding to the lane markings. The lateral offset values of these points from the median crash barrier were used to differentiate them into four lane marking groups. This process is shown in Figure 2.9.

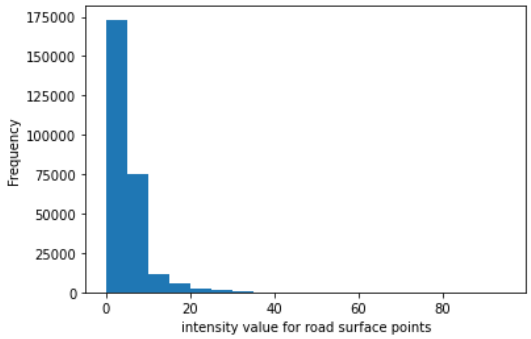

Figure 2.8. Histogram of road surface intensity values

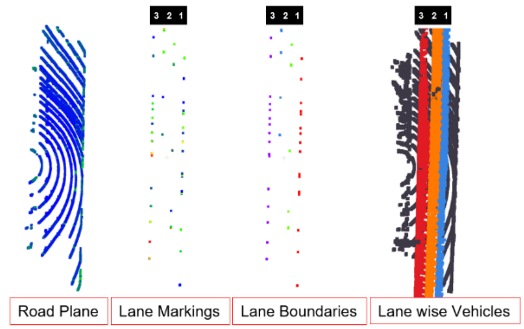

Figure 2.9. Road Plane, Lane Markings and Lane Wise vehicles

The descriptive statistics of all four groups of lane mark points are shown in Table 2.2.

Table 2.2. Descriptive Statistics of Lane Marking offsets from Median

	Lane Marks 1	Lane Marks 2	Lane Marks 3	Lane Marks 4
count	1104	106	95	520
mean	7.63	19.31	31.00	42.57
std	0.03	0.05	0.06	0.05
min	7.91	19.73	31.72	43.08
25%	7.70	19.41	31.02	42.65
50%	7.63	19.23	30.93	42.56
75%	7.55	19.18	30.88	42.47
max	7.27	19.10	30.82	42.26

The first lane boundary was 7.91 feet from the median and the farthest lane boundary was 43.08 feet from the median. Also, the lane widths from these offsets were estimated to be 11.8ft, 11.99ft and 11.36ft respectively. These estimated lane boundary offsets were used to split and assign the vehicular point clouds into their corresponding lanes as shown in Figure 2.9.

2.4. Lane Based Object Detection and Volume Counting

The vehicular point clouds from each frame were obtained from the raw scans of point clouds after eliminating the static background points using the lower bound of the farthest radial distance background mask estimated in section 2.2.2. These vehicular point clouds consist of all the vehicular objects present in the LiDAR detection Zone at that moment. To derive individual vehicle attributes, it is necessary to group the points of the same vehicle together. For this purpose, use the Density-based Spatial Clustering of Applications with Noise (DBSCAN) from Li, Y et al.(*24*) was continued.

The DBSCAN clustering algorithm takes two parameters as input. The first one is the radius of search within which the algorithm searches for neighboring points, and the next is the minimum number of neighboring points that needs to be used as a threshold in that neighborhood with the specified radius. The algorithm estimates the density of each point based upon the number of points present within the specified radius and clusters those with similar neighborhood density. The lane-based object detection results for a randomly selected frame at I-710 are shown below in Figure 2.9. A radius of 13.12 ft was used to search for the neighborhood, considering that the I-710 corridor would have heavy duty trucks of different body configurations passing through the detection zone. The requirement for the minimum number of points was set as 100, considering that the detection zone can be significantly widened when a smaller threshold is applied.

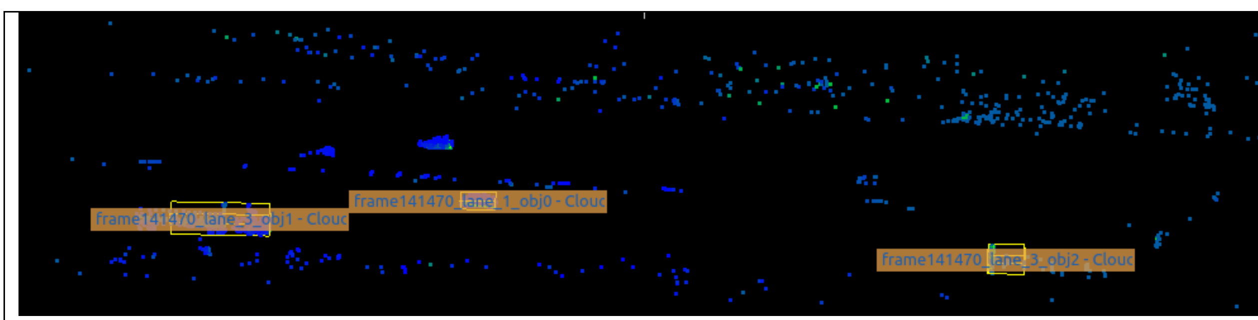

Figure 2.10. Lane based object detection results for Frame 141470 at I-710

2.4.1. LiDAR virtual loops and Lane based volume counts.

One important traffic parameter to be obtained from the LiDAR sensor is vehicle count. To get volume counts from the LiDAR sensor, a virtual loop was set up at the same location as the Truck Activity Monitoring System (TAMS)(*16*) inductive loops installed on I-710. The leading edge and trailing edge of TAMS loops are located at 49.2 ft and 55.8 ft along the travel lane (y-axis of LiDAR scan zone) upstream of the LiDAR location.

The position of the leading edge of a vehicle's LiDAR single scan was used to actuate the virtual loops in the LiDAR detection area. Vehicles leading edge, trailing edge, and both sides are estimated by computing a minimum oriented bounding box for the LiDAR scan of vehicle(*26*). The I-710 corridor can have vehicles traveling at very high speed during the night time and hence a threshold bound-based position of the leading edge was used to actuate the LiDAR virtual loop. Assuming that the fastest vehicle would be at 100mph speed, it would cover 14.67 ft during 0.1 seconds of the LiDAR frequency, hence the combined 55.8+14.67 = 70.47 ft to 55.8 ft upstream region was defined as the activation region of the LiDAR's virtual loop. This is illustrated in Figure 2.11.

2.4.1.1. Dataset, Volume Counts, and Comparison with TAMS Data

The volume count of vehicles was conducted for a 4-hour LiDAR dataset collected at I-710 on 5th May 2022 from 8pm to midnight.

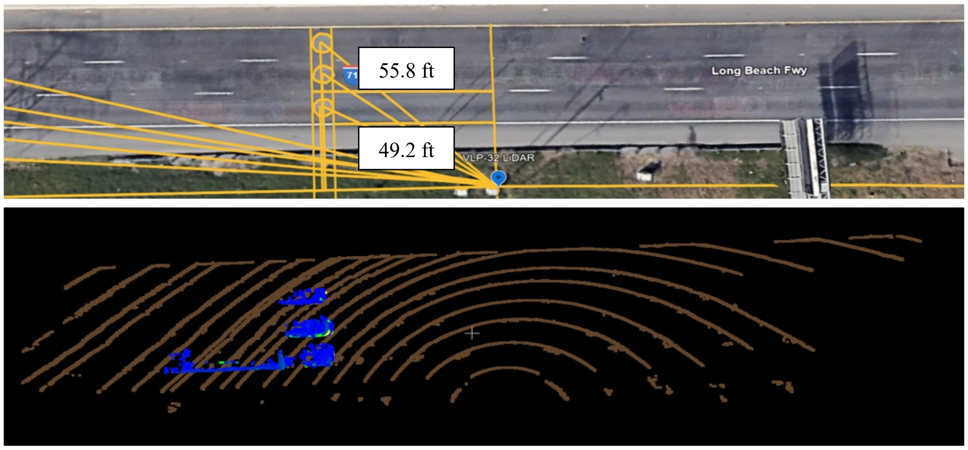

Figure 2.11. Location of ILD and corresponding LiDAR virtual loops at I-710

The attributes of traffic that are recorded when the LiDAR's virtual loop is activated are shown in Table 2.3. It consists of the timestamp of actuation, lane of actuation, the lateral distances of the vehicles bounding box, the longitudinal distances of leading and trailing edges of the vehicle along with its width and length. The timestamp information along with lane of actuation can be used to obtain the desired time interval volume counts of 30-seconds or 5-minutes or 15-minutes.

Table 2.3. Attributes of Traffic captured by actuation of LiDAR virtual loops.

Frame	Time Stamp	Truck	Lane	obj	Minimum Lateral Distance (ft)	Maximum Lateral Distance (ft)	Distance of Front Edge (ft)	Distance of Trailing Edge (ft)	width (ft)	Length (ft)
34	8:00:05 PM	1	2	0	38.74	44.27	64.92	78.42	5.38	13.44
50	8:00:07 PM	2	2	0	37.35	43.14	65.32	79.43	5.45	13.99
64	8:00:08 PM	3	1	0	50.42	56.37	67.64	86.79	5.86	19.12
67	8:00:08 PM	4	2	1	37.87	43.73	67.06	81.22	5.80	14.13
104	8:00:12 PM	6	2	0	37.58	45.64	62.37	130.32	7.37	67.88

2.4.1.1.1. Truck Activity Monitoring System (TAMS)

TAMS is an ILD-based system mainly developed for the detection and classification of heavy-duty vehicles but it provides highly accurate information of all FHWA classes of vehicles from 2 to 13 along with the body classification as well (*16*). The volume counts obtained by TAMS during 5th May 2022 from 8pm to midnight were used to compare with the volumes obtained from the actuation of the LiDAR virtual loops. For the three lanes, the 15-minute volume count comparisons are provided in this section.

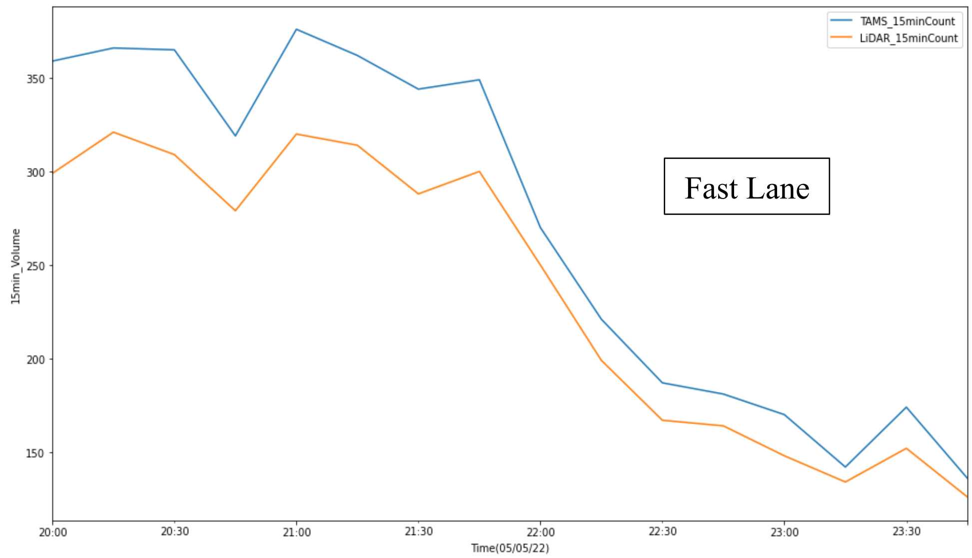

Figure 2.12. 15-minute volume counts (TAMS vs LiDAR) for Fast Lane

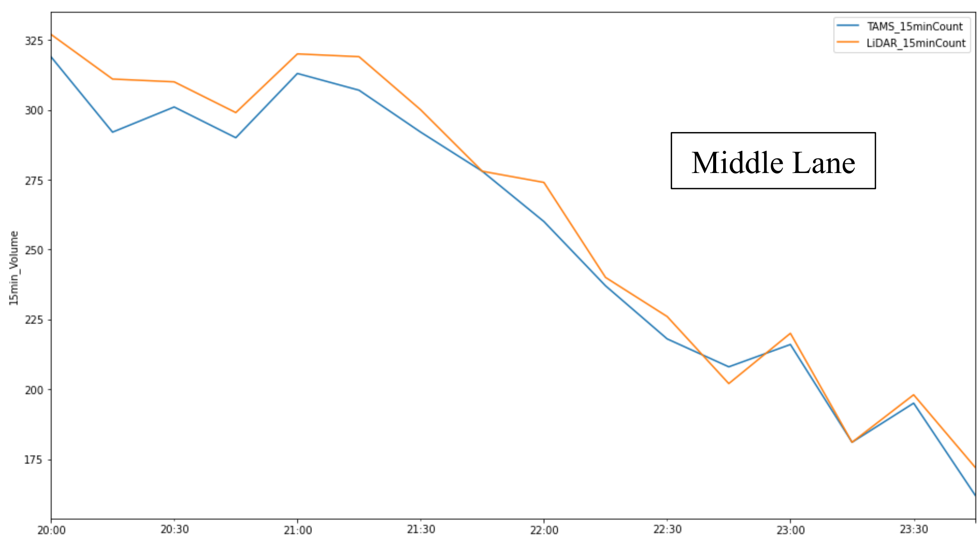

Figure 2.13. 15-minute volume counts (TAMS vs LiDAR) for Middle Lane

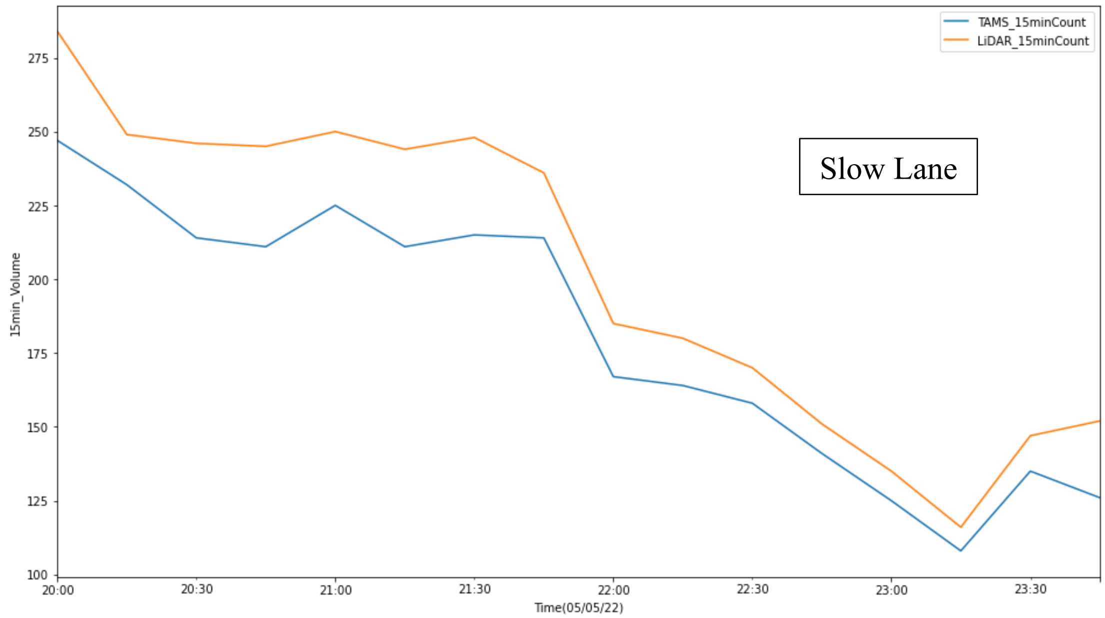

Figure 2.14. 15-minute volume counts (TAMS vs LiDAR) for Slow Lane

Table 2.4. 4-hour volume counts TAMS vs LiDAR at I-710

Date	Lane	Lane Type	TAMS Count	LiDAR Count	Percentage
5/5/2022	1	Fast	4321	3770	87.2
5/5/2022	2	Middle	4069	4177	102.7
5/5/2022	3	Slow	2893	3238	111.9

Overall LiDAR volume counts in the fast lane were estimated to be 87.2 percent of the TAMS counts and these numbers are in line with engineering judgement as vehicles in the fast lane might be occluded by vehicles passing through the middle lane or slow lane.

The LiDAR volume counts for the middle and slow lanes were higher than that of TAMS. This could be due to one or more of the following reasons. (1) The possibility that object detection is creating double counts of the same vehicle pertaining to the tracking done using the Kalman filter algorithm, or (2) the loop count missed a vehicle passing by whereas LiDAR captured the instance of the vehicle. The first point can be addressed by increasing the accuracy of LiDAR object detection by employing other variants of Kalman filter.

2.4.1.2. Medium and Heavy-Duty Vehicle Volume Comparison

As shown in Table 2.3, the width of a vehicle and its length in travel direction were two of the attributes collected when LiDAR virtual loops were actuated. The length distribution of the vehicles that actuate the LiDAR virtual loop can be used to perform a crude classification of vehicles into medium and heavy-duty vehicles, as their length tends to be greater than 16.54 ft.

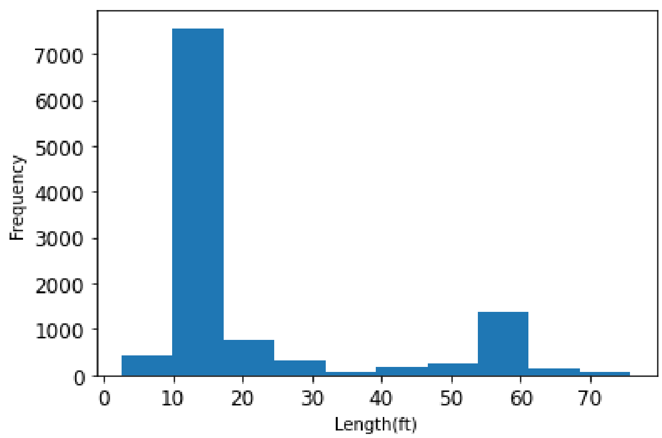

Figure 2.15. Vehicle Length (ft) distribution at the LiDAR virtual loops

A Gaussian Mixture Model (GMM) based clustering technique was applied to vehicle length to separate medium and heavy-duty vehicles from passenger vehicles. GMM clustering identified 35% of the vehicles to be medium and heavy-duty vehicles.

Table 2.5. Descriptive statistics of Length (ft) for two GMM clusters

	Passenger Vehicles (ft)	Non-Passenger Vehicles (ft)
count	7278	3907
mean	13.74	37.86
std	0.96	20.31
min	10.85	2.59
25%	13.18	18.2

50%	13.72	43.14
75%	14.32	57.2
max	16.54	75.89

The descriptive statistics of the length in feet for both clusters of the vehicles at LiDAR virtual loops is presented in Table 2.5. Based on this, the medium and heavy-duty vehicle volume counts at LiDAR virtual loops were compared with TAMS counts. For presentation purposes, the 30-second volume counts between 8:00 pm and 8:30 pm on 05th May 2022 are shown.

From the 30-second MHDV volume count figures, LiDAR volume counts are larger than TAMS volume counts in multiple instances. Approximately 10% of such instances from LiDAR were manually verified to make sure non-vehicular objects were not present in the data. One such 30-second instance where the TAMS count was 4 vehicles and LiDAR virtual loop count was 8 vehicles is shown in the figure below.

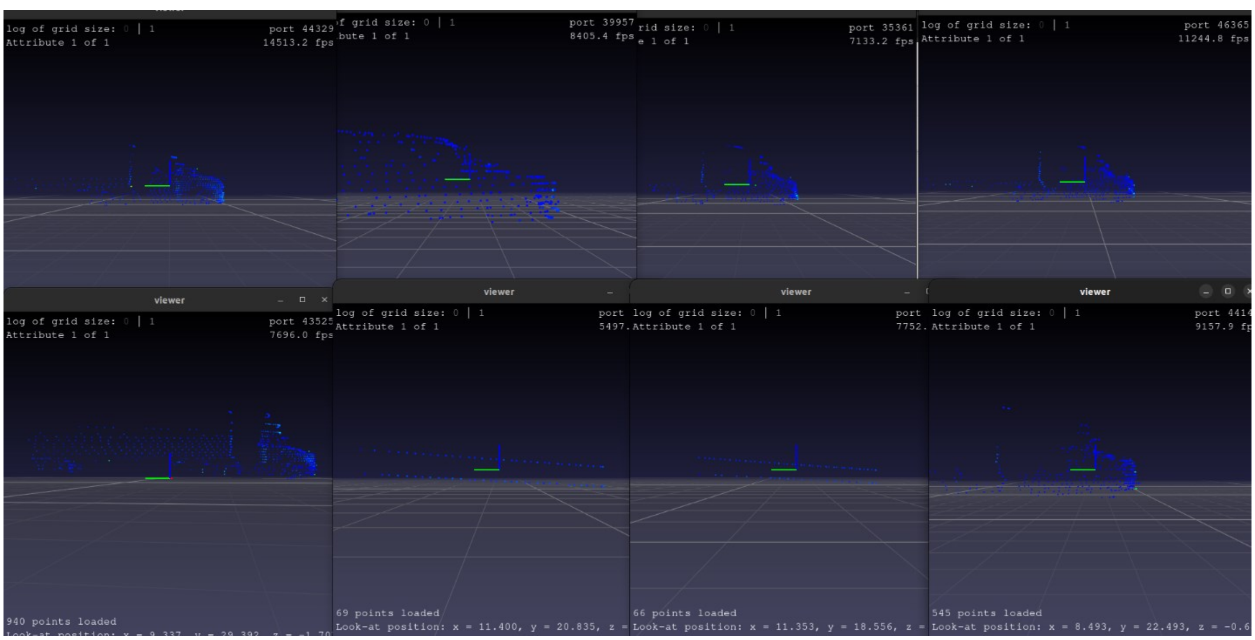

Figure 2.16. A 30-second instance in which LiDAR volume count is 8 and TAMS count is 4

From Figure 2.16, the 2nd and 3rd vehicles in the bottom row most likely belong to the same vehicle and are double counted. Also, the number of points present in each of the frame is so less, it indicates the DBSCAN clustering probably removed some vehicle points as noise. If both these objects are counted as one or even if ignored completely, the LiDAR virtual loop still detects more vehicles than TAMS and no other vehicle was a double count, as they were completely different to the consecutive vehicles. This finding is valuable and warrants further research on to why TAMS is missing the vehicle while LiDAR is still capturing it.

The 30-second volume count of medium and heavy-duty trucks across three lanes are presented in Figure 2.17 to Figure 2.19. From these figures two interesting inferences can be made. The first one illustrates there is scope to improve the object detection process of LiDAR sensor and the second inference is that LiDAR has potential to perform at par or better with respect to loop detectors if the object detection works 100% accurately. Both the inferences need to be quantitatively established but this work asserts positively in that direction.

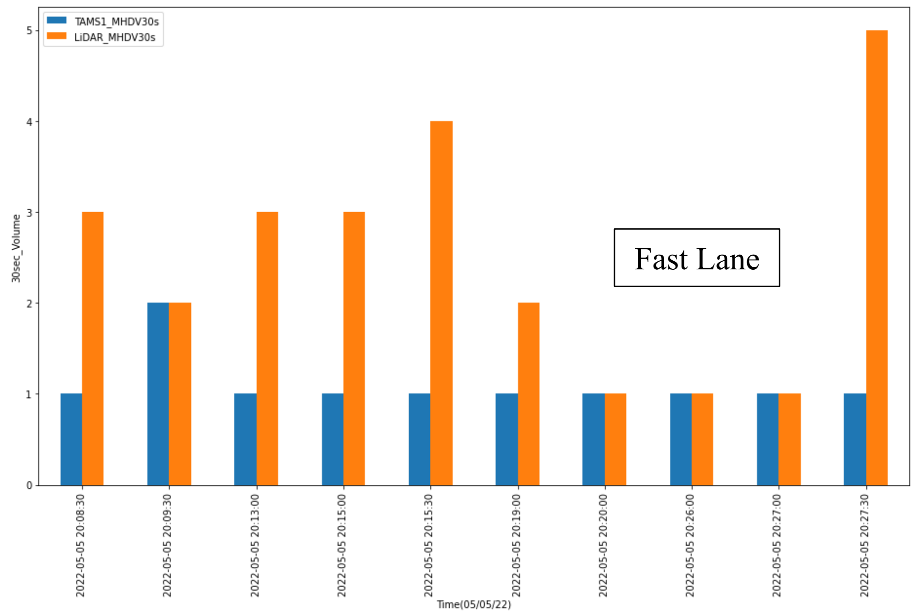

Figure 2.17. MHDV volume comparison for Fast Lane

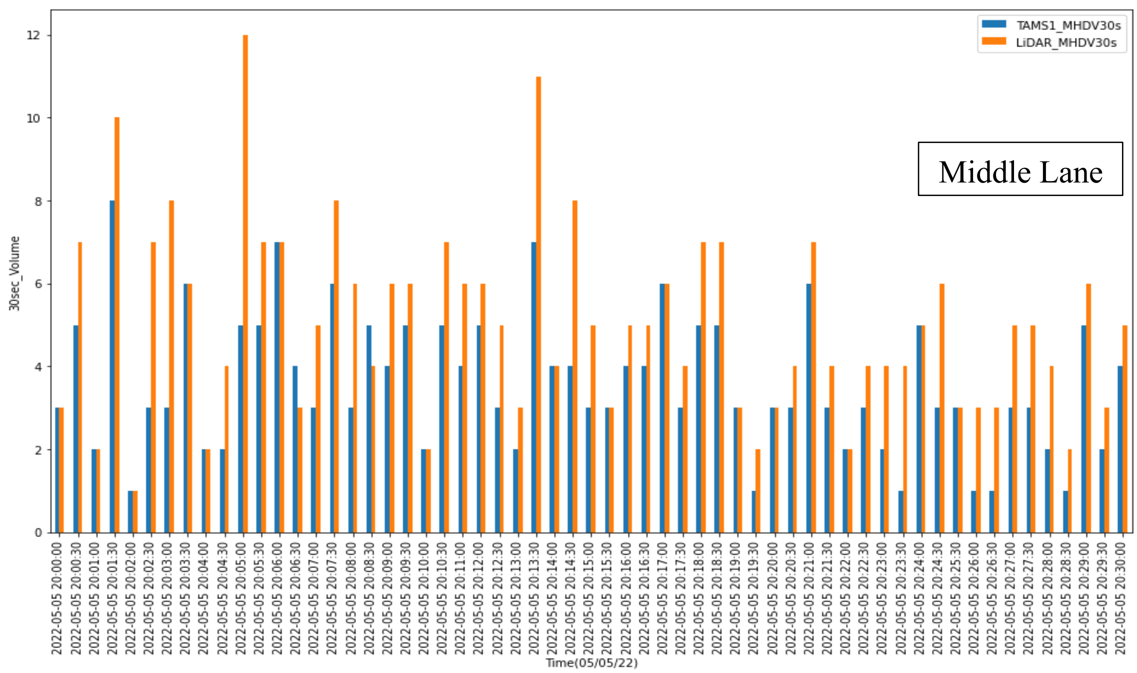

Figure 2.18. MHDV volume counts for Middle Lane

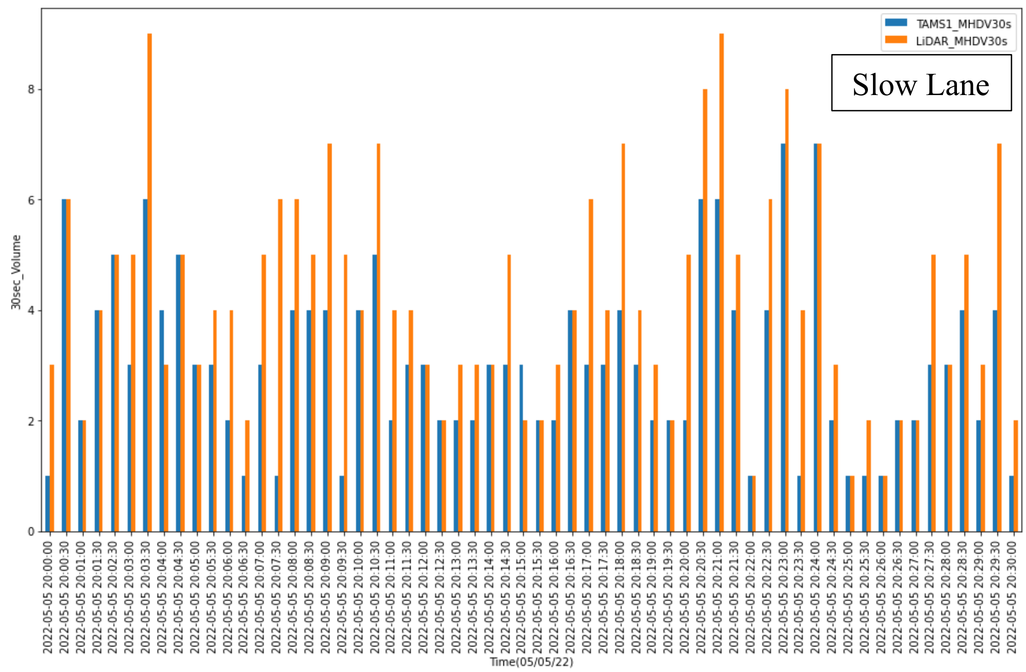

Figure 2.19. MHDV Volume Counts for Slow Lane

2.5. Conclusion

Chapter two has presented a novel lower bound of farthest radial distance-based background subtraction algorithm and automatic lane-based object detection pipeline. Traffic volumes on a three-lane dense urban traffic corridor are estimated using LiDAR virtual loops and compared with TAMS. The LiDAR's virtual loops capture and record the lateral distances of vehicle's sides and longitudinal distances of the leading and trailing edges of vehicles as well as their width and length. Thus far, the traffic parameters are derived using individual scans of vehicles passing through the LiDAR detection zone. To derive other traffic parameters such as actual physical dimensions of vehicles, microscopic trajectories, and actual three-dimensional positioning within lanes, it is necessary to group individual scans of the same vehicle and reconstruct. Chapter three describes the same.

3. LiDAR Data Association, Tracking and Reconstruction

3.1. Introduction

The individual LiDAR scans of a vehicle comprise partial body point clouds as it was passing through the LiDAR scan area and each LiDAR scan can consist of multiple vehicles at a given instant. The partial body point clouds of same vehicles from successive LiDAR should be mapped and grouped together for any other traffic parameters to be obtained. The process of mapping and grouping partial body point clouds of same vehicle is achieved by data association and multiple object tracking algorithms. Once the grouping is accomplished, the partial body point clouds of the same vehicle are subjected to multiway registration for developing a point cloud that comprises all the details of vehicle as it is passing through the point cloud.

The current chapter utilizes all the scans of a truck while it is passing through the detection zone of a roadside mounted 32 beam Lidar sensor rotating 180 degrees in horizontal field of view. The grouping of LiDAR point clouds of same truck is done using Hungarian Algorithm based data association in conjunction with Kalman filter based multiple object tracking.

The full body of truck passing through LiDAR detection area can be reconstructed to obtain the actual geometry of truck. For this purpose, we formulated a two-stage truck body reconstruction framework using all the roadside LiDAR scans of truck while it was in the detection zone. During the first stage a pairwise LiDAR point cloud registration is performed and in the second stage all the point clouds are transformed to a global coordinate framework using Simultaneous Localization and Mapping (SLAM) based optimization.

The rest of the chapter is organized as described here. Section 3.2 presents the existing literature for addressing our problem. Section 3.3 presents the framework used for reconstructing the Truck bodies which can further be used for vehicle classification purposes. Section 3.4 presents qualitative and visual results for various types of reconstructed trucks.

3.2. Literature Review

A LiDAR sensor captures the 3D points of the target along with corresponding intensity values in its scanning zone. Point cloud registration is aligning two such scans of a target and mainly draws its motivation from range image registration. Point cloud registration is an important and challenging problem in domains such as computer vision, medical image processing, robotics, self-driving/intelligent vehicle applications(*27*), photogrammetry, remote sensing, environmental monitoring, etc. In medical imaging multiple images by computer tomography or magnetic resonance imaging are fused using feature-based registration. In remote sensing Lidar-based registration is mainly used for forest parameter estimation, land cover classification, solar energy potential estimation, natural disaster monitoring, and water surveys etc.(*28*). In computer vision, registration is used for localization and mapping purposes as well as indoor scene reconstruction which is useful for virtual reality and augmented reality-based applications.

Initial formulation of point cloud registration was proposed by Besl and McKay (*29*) and the problem is described as aligning the 3D data of an object scanned in a sensor coordinate system to a model shape (3D data) represented in a model coordinate system by iteratively estimating optimal rotation and translation parameters, which minimizes the point-to-point distance between both datasets (*30*). This is called the iterative closest point algorithm and is widely used for LiDAR point cloud registration. The ICP algorithm has six stages and needs an initial set of parameters. The original ICP algorithm is sensitive to the initialization of parameters and requires good overlap between the scan and model object to obtain tight alignment. To overcome this several variants of ICP have been proposed as discussed in (*31*).

Another widely adopted strategy for the point cloud registration is coarse-to-fine registration strategy. In coarse registration, initial registration parameters for the two-point clouds are estimated using some derived features of the point clouds. Generally, point based, or line based, or surface-based features are derived for coarse registration purpose. In fine registration the maximum overlap between both point clouds is achieved using either an iterative approximation method or normal distribution transformation method. The general point-based features extracted are point feature histograms, fast point feature histograms, heat kernel signature, mesh-difference-of-gaussians etc. (*28*). Salvi, J et al., (*32*) analyzed and provided a comprehensive review of both coarse and fine registration methods. As per their findings, a RANSAC-based coarse registration yielded better results, and they also showcased the local minima problems present in the original formulation of ICP by Besl and McKay. The coarse-to-fine registration strategy is well suited when one only needs to do registration for a couple of point clouds. For several applications such as indoor scene reconstruction multiple point clouds might need to be aligned together to confirm to a global coordinate system. Zhu, H et al., (*27*) provided a detailed review of both pairwise as well as Groupwise registration methods. They conducted experiments on 10 representatives of pairwise as well as groupwise registration algorithms. Their work found a probability based Coherent Point Drift (CPD) method is found to perform better for pairwise registration.

While the literature found a wide variety of algorithms for registration purposes, this research tested the multiway registration framework presented in Open3D (*33*). The results from this are qualitatively assessed and presented in section 3.4

3.3. Methodology

In the current framework a two-stage truck body reconstruction framework is developed to obtain a comprehensive scanned body of a truck passing through the side-fire Lidar Detection Zone (LDZ). In the first stage, a sequential pairwise rigid transformation matrix was estimated using a coarse-to-fine registration strategy. In the second stage, global optimization was performed on a pose graph (a graph with nodes and edges in which each node represents the posture of an object and each edge defines the relation between its connecting postures.) constructed using the sequential pairwise transformation matrices from the first stage to construct the merged point cloud. The proposed framework is shown in Figure 3.1. below.

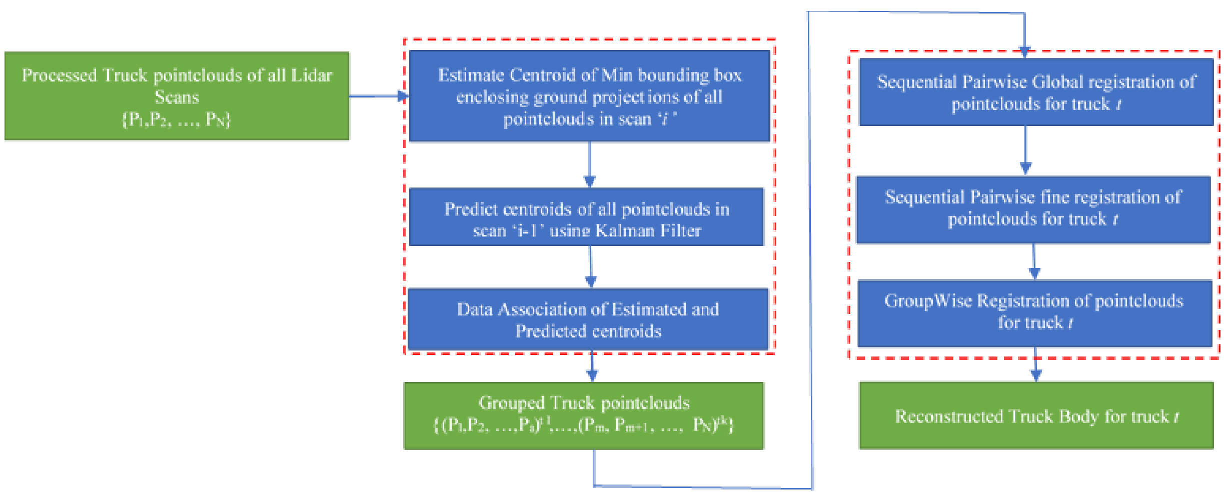

Figure 3.1. Proposed 2-Stage Truck Body Reconstruction Framework

3.3.1. Experimental Setup and Data Collection

A 32-beam Velodyne LiDAR was set up adjacent to the shoulder of truck scale lane on Southbound I-5 at a California Highway Patrol facility near San Onofre, California. LiDAR scanning was restricted to 180 degrees horizontal field of view and scanned at a frequency of 10 HZ. Data was collected for a duration of approximately 134 hours over twelve days.

The raw point clouds obtained from the Lidar were processed using DBSCAN to remove the background and statistical outliers as proposed in (*22*). Each scan of the side-fire Lidar sensor captured all the truck bodies partially present in LiDAR's Detection Zone (LDZ). The scans had rich information of the front portion of a truck entering the LDZ, the side of the truck when it is in the midsection part of the LDZ, and the rear portion of the truck when it is leaving the LDZ. A more detailed truck body can be reconstructed by aggregating all its point clouds captured while traversing the LDZ, as illustrated in Figure 3.7

3.3.2. Object Tracking and Data Association

For creating the aggregated and comprehensive truck body, it is necessary to track and map the scans corresponding to the same truck from all the scans while the truck is present in LDZ. Object tracking is a problem of estimating the trajectory of an object of interest from frame to frame in a LiDAR video scene. Object tracking is generally preceded by an object detection algorithm for the objects of interest. A tracking algorithm would achieve this objective by assigning consistent labels to the tracked object in different frames of the LiDAR scans. Object tracking is inherently complex due to occlusion and complex interactions of objects.

Based on how objects are represented, the tracking can be done point based, kernel based, or silhouette based. In transportation applications, objects can be tracked as bounding boxes using network-based Bayesian filtering algorithms such as Kalman filter or Particle filter. They work quite well for single objects, but in the presence of multiple objects the tracking problem expands into another dimension of data association (correspondence) along with tracking. Two popularly used multiple-object tracking algorithms are Joint Probability Data Association Filtering (JPDAF) and Multiple Hypothesis Tracking (MHT) but their computational complexity grows exponentially(*34*, *35*). Bewley et al, (*17*) proposed a very efficient framework of using Hungarian Algorithm and Kalman filter for multiple-object tracking.

Kalman Filter (KF) is a recursive filter that estimates the hidden states of a linear dynamic system from a series of noisy measurements. KF is analogous to Hidden Markov Model except that the state variables of KF are continuous. KF can estimate the velocity and acceleration of moving objects, given a noisy measurement of object's state(*36*).

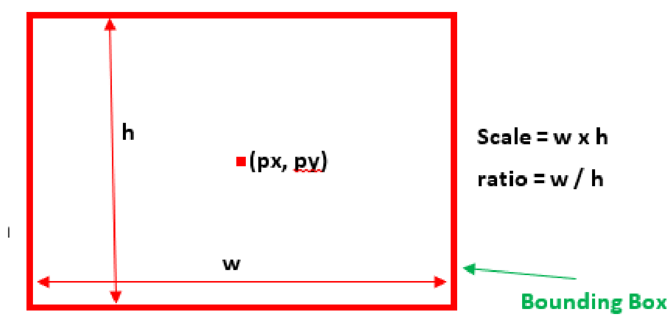

Figure 3.2. Bounding box and state variables

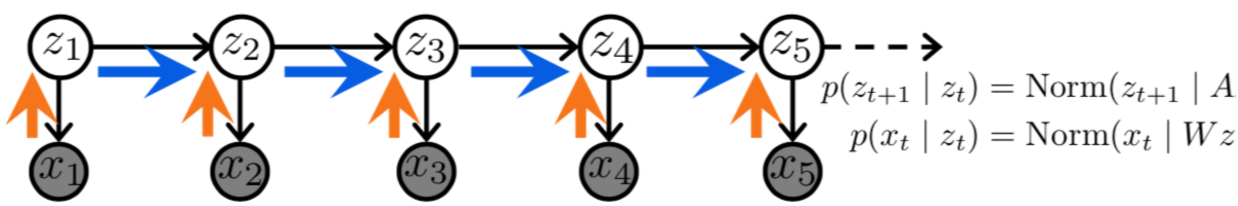

Figure 3.3. Kalman filter schematic representation

Processed truck object scans in successive frames would be tracked using the Simple Online Real Time Tracking (SORT) as proposed by Wozke, N et al., (*37*). The centroid of the minimum oriented bounding box of 2D ground projection of the truck was used as the state variable for tracking purposes. Multiple object tracking is carried out using a constant velocity based Kalman Filter, as shown in Figure 3.5 below. The predictions from the previous scan and estimations from the current scan of the state variables were mapped to each other using a Hungarian Algorithm(*17*). This framework is designed to keep predicting and updating the Kalman Filter state of missed detections for up to 5 consecutive scans. There are several Multiple-Object Tracking algorithms developed in the literature, but the current framework was chosen as it performs quite well in a real time tracking context (*17*).

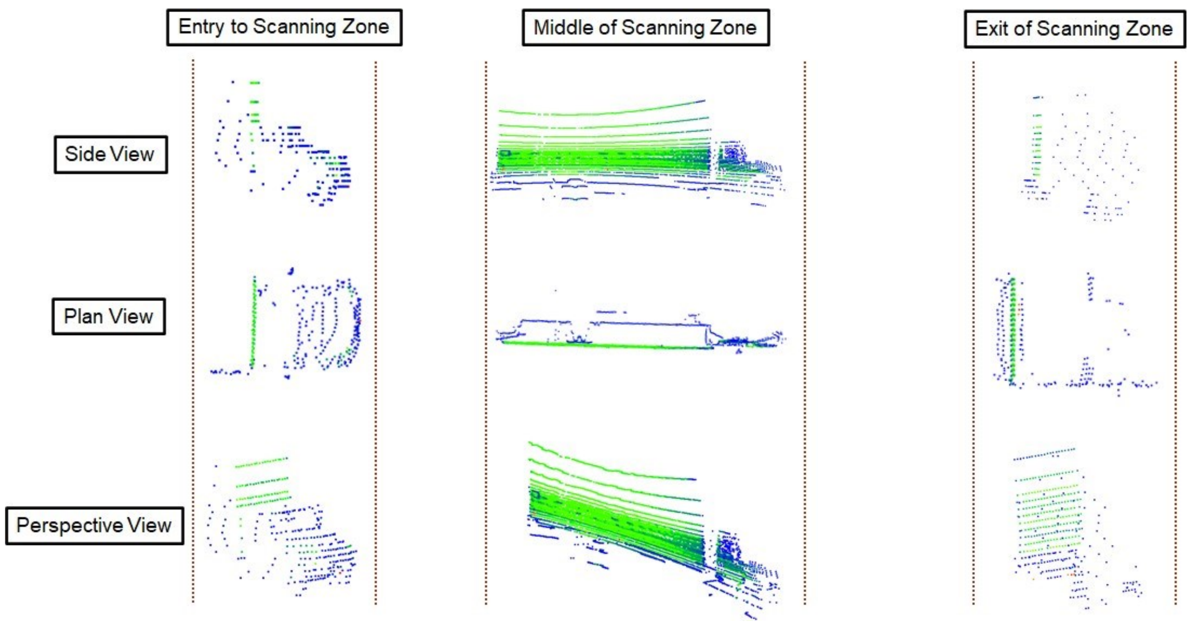

Figure 3.4. Truck Scans at different parts of LDZ

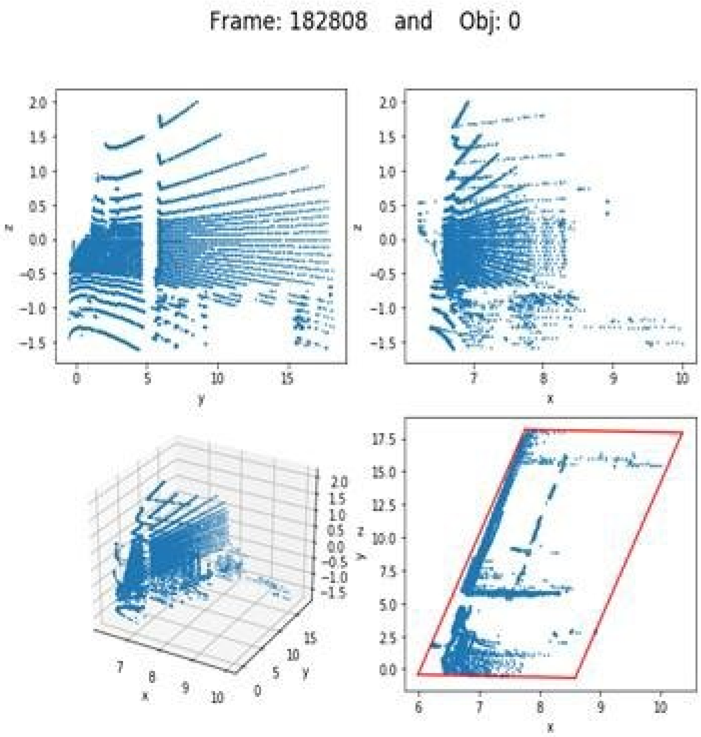

Figure 3.5. Minimum Oriented Bounding box for ground projected Truck Scan

3.3.3. Sequential Pairwise Registration

A coarse-to-fine registration strategy was adopted to obtain the sequential pairwise rigid transformation matrices for each pair of truck point clouds. An initial estimate of the rigid transformation matrix was estimated using fast point feature histograms (fpfh) and the RANSAC algorithm. The output from RANSAC was used as initialization for the standard ICP algorithm and finetuned for tighter alignment. This is illustrated in Figure 3.6 below.

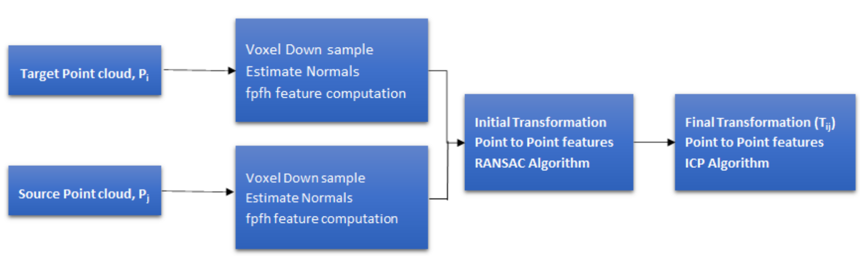

Figure 3.6. Sequential Pairwise Coarse-to-fine registration framework

3.3.4. Truck Body reconstruction using Pose graph Optimization.

The sequential pairwise transformation matrices along with the corresponding point clouds were used to construct a pose graph. This pose graph was optimized to align all the point clouds globally and merge with a reference point cloud of truck while it is in the mid-section of the LDZ. The SLAM based optimization framework proposed in Choi et al., (*38*) was used in this framework. Construction of the pose graph and the merged point cloud are schematically shown in Figure 3.7.

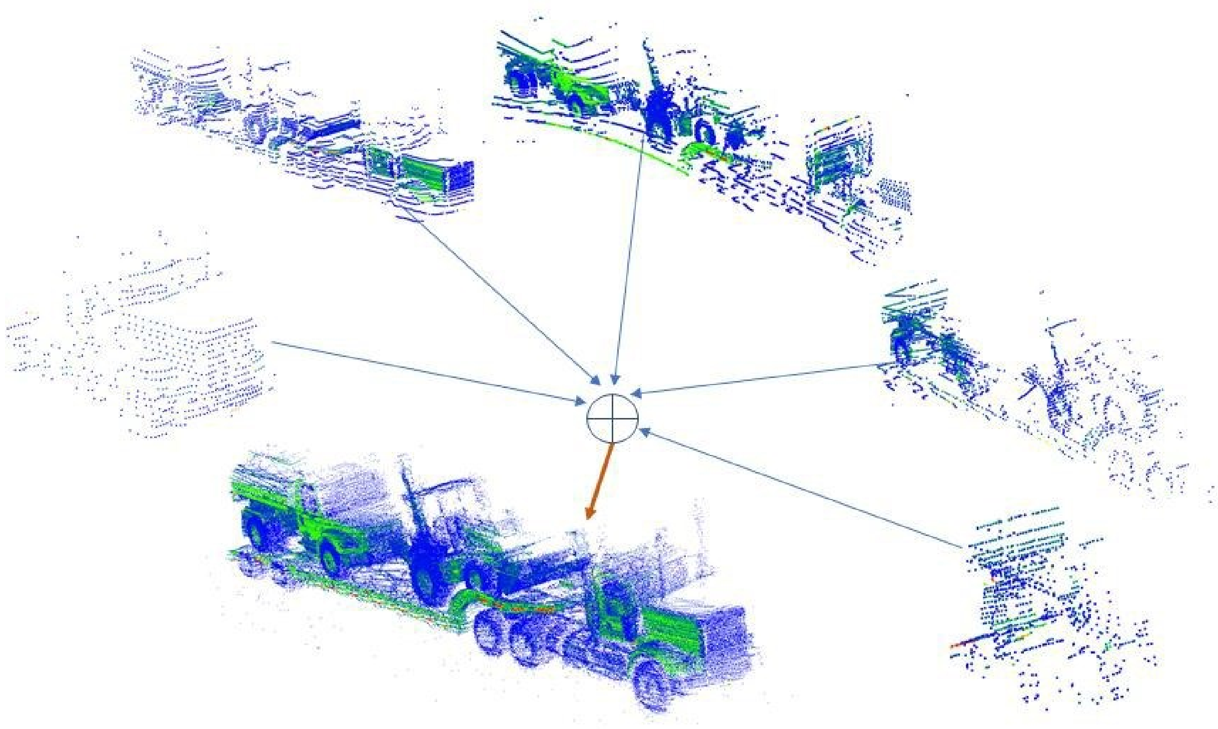

Figure 3.7. Schematic Representation of Pose Graph-based Truck body Reconstruction

3.4. Results and Discussion

Qualitative results from the truck body reconstruction results for 9 types of truck-trailer combinations are presented in this section. The results are reasonably similar for other additional truck-trailer configurations identified in (*3*). Those results were also verified visually but not presented here for the sake of brevity.

For the 9 types of truck-trailer configurations provided, except for the 40 ft and 53 ft container trailers, the reconstructed truck bodies look quite intact. For the 40 ft and 53 ft trailers, qualitative assessment reveals that the sparse presence of points in the lateral direction could be causing the reconstructed body to be slightly misaligned at the wheels. This is proposed to be investigated in future work.

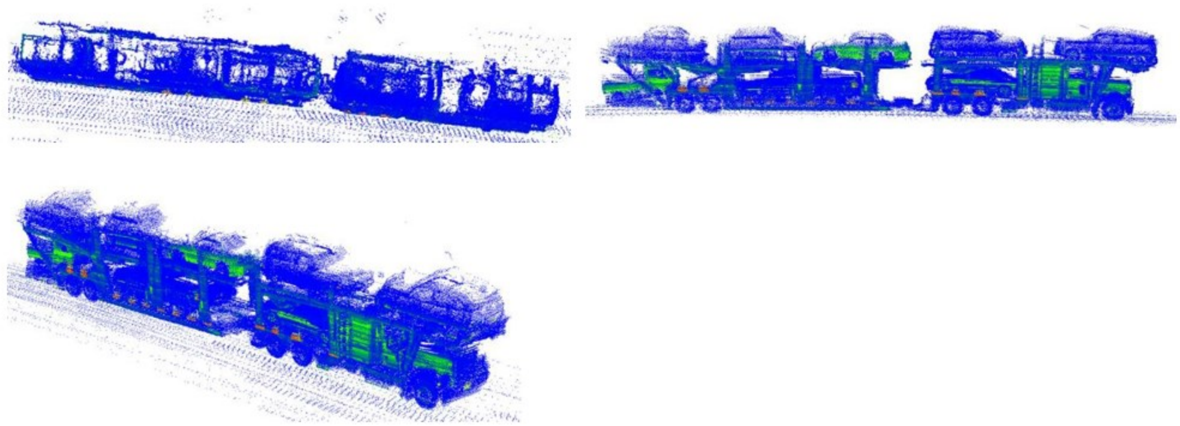

Figure 3.8. Automobile Transport

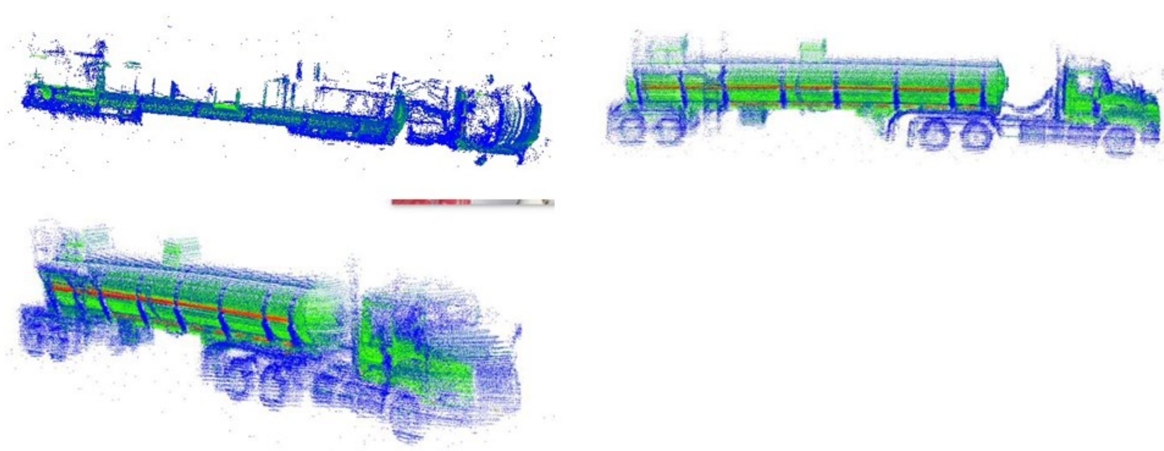

Figure 3.9. Tank Trailer

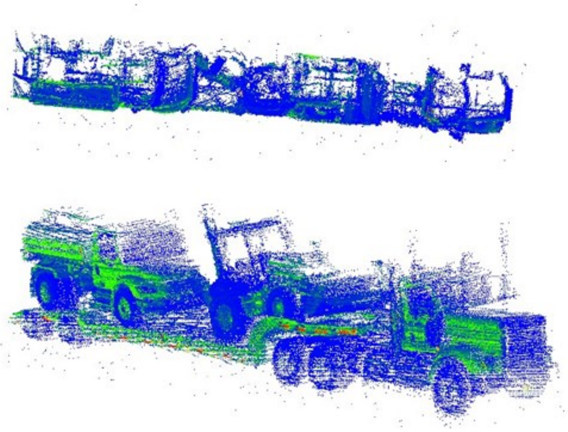

Figure 3.10. Low Boy Platform

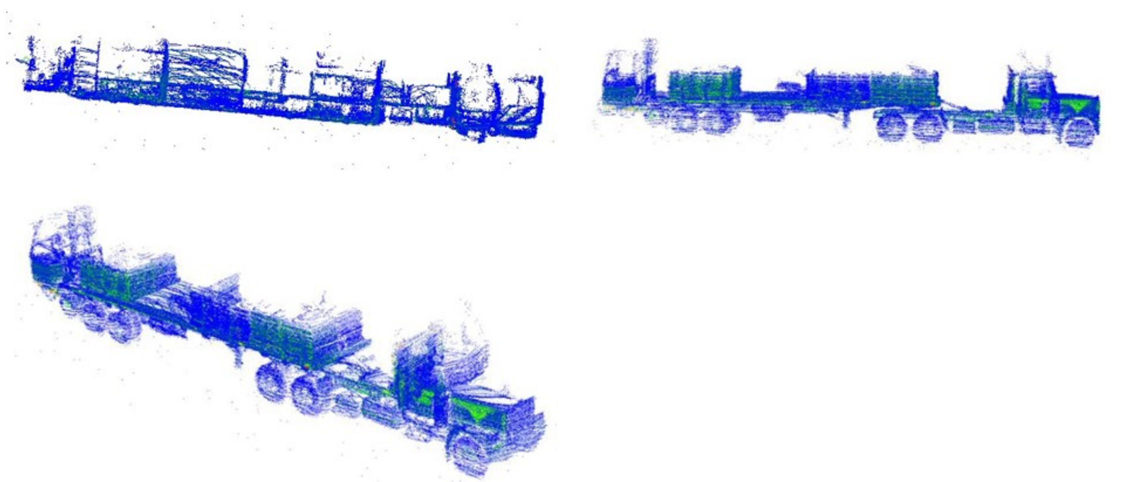

Figure 3.11. Basic Platform

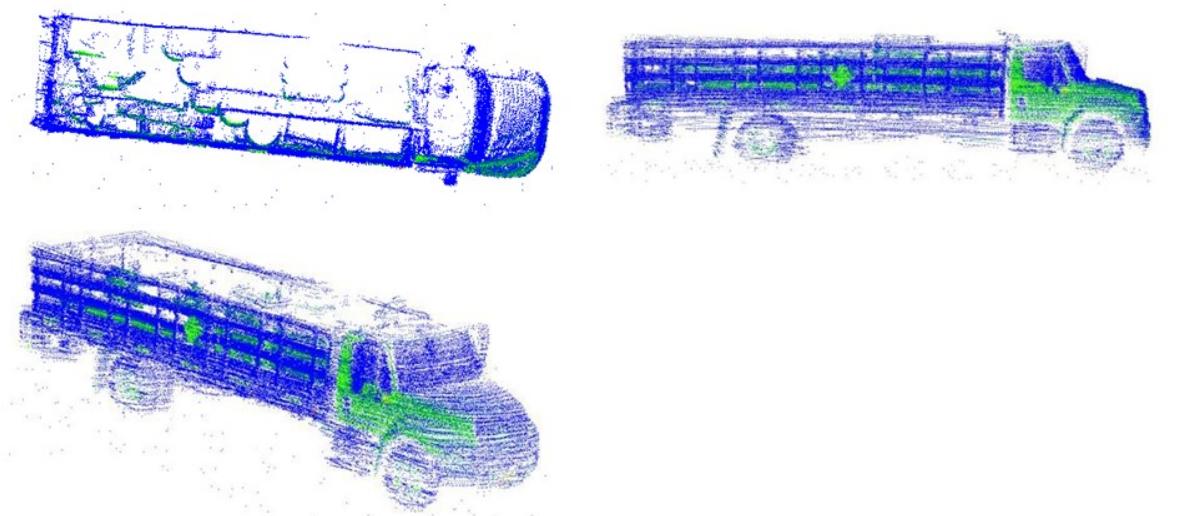

Figure 3.12. Stake Body Truck

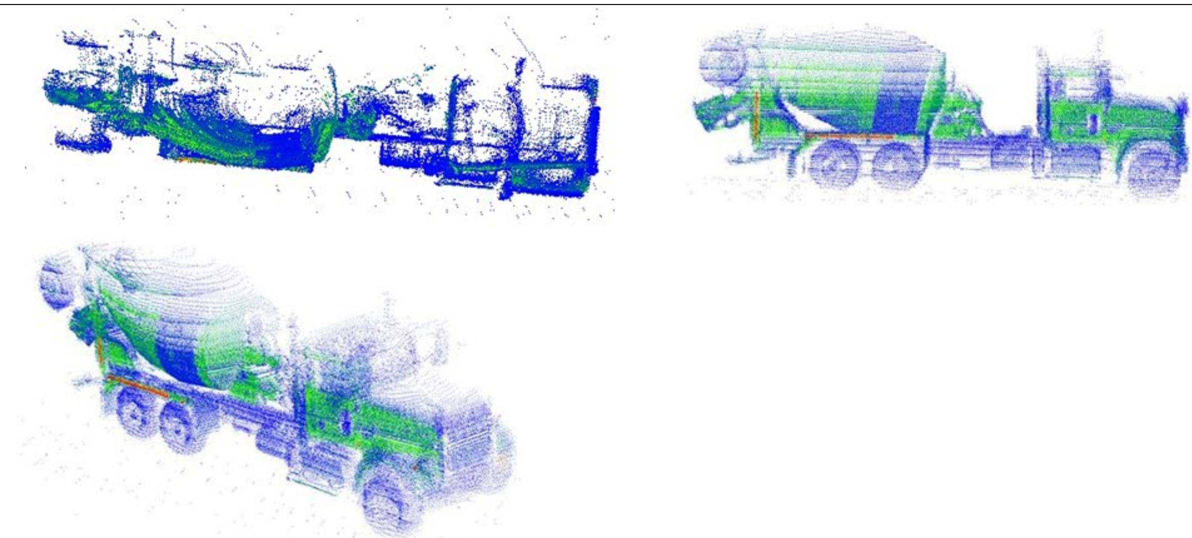

Figure 3.13. Concrete Mixer Truck

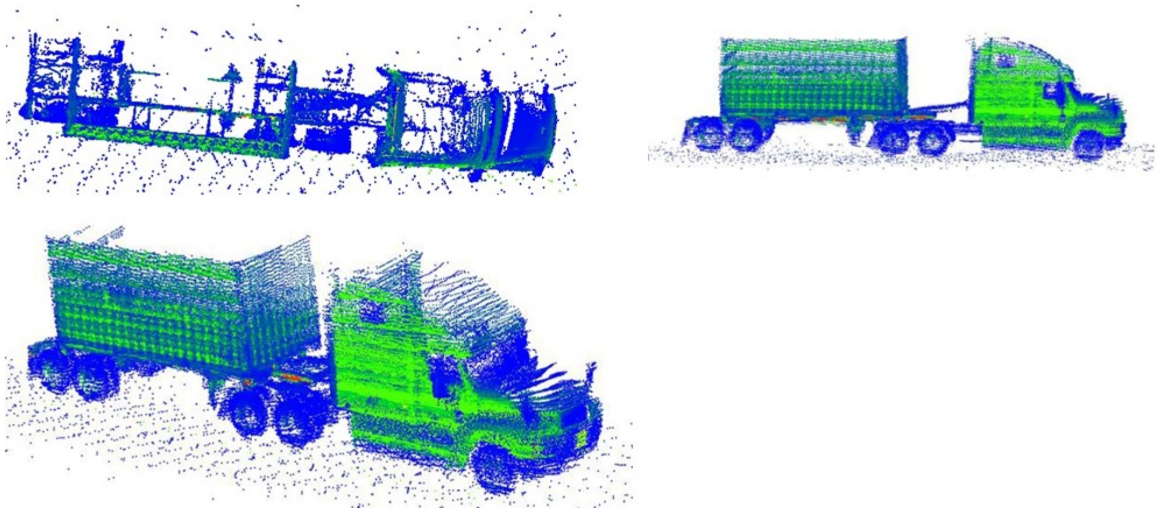

Figure 3.14. 20 feet Drayage Container

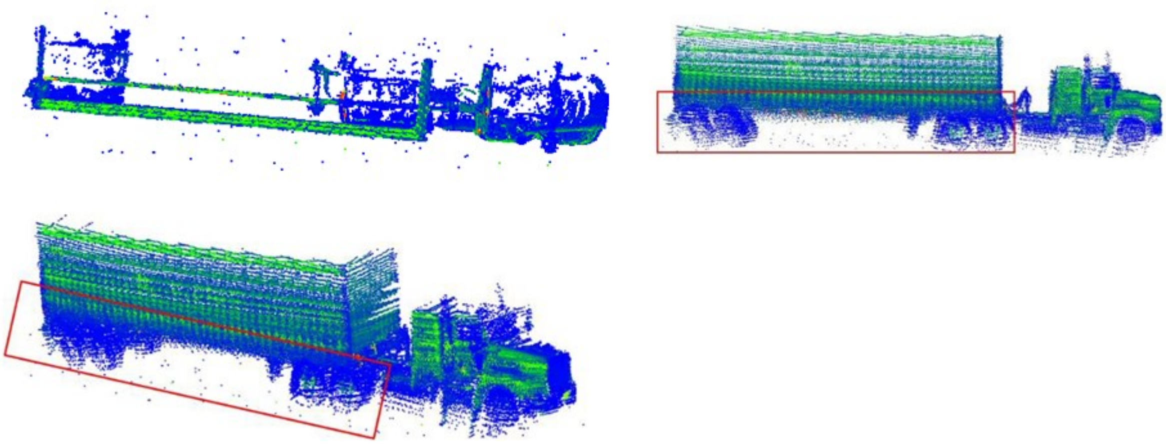

Figure 3.15. 40 feet Drayage Container

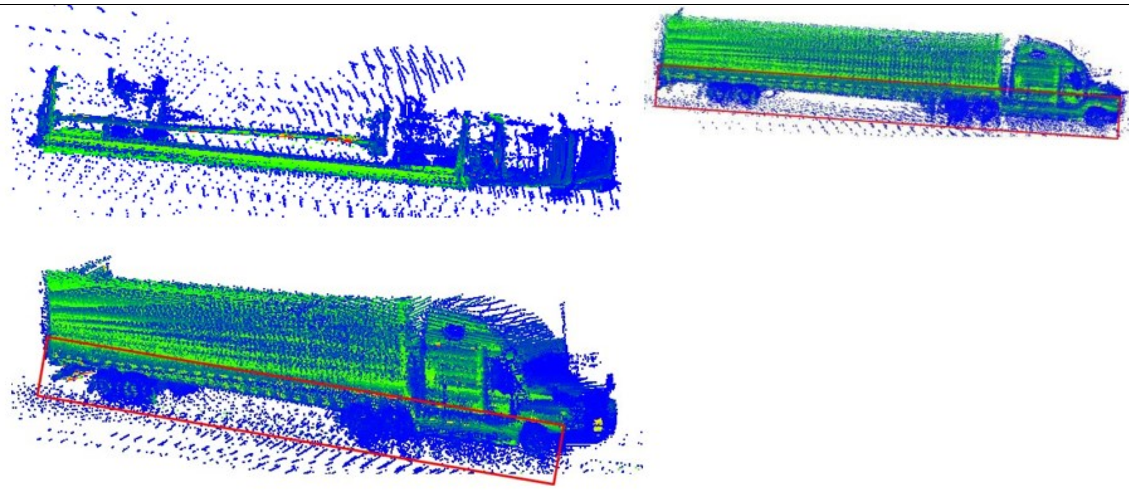

Figure 3.16. 53 feet domestic intermodal container

3.5. Conclusion

This chapter presented a LiDAR-based reconstruction framework for truck surveillance purposes. The reconstructed truck bodies could play a vital role in developing commercial vehicle activity monitoring applications such as body classification, axle-based classification, network level commercial vehicle tracking, etc. The presented framework consisted of two stages where in the first stage the lidar scans corresponding to the same trucks were grouped together using a Kalman Filter and Hungarian Algorithm. During the second stage a combination of sequential pairwise coarse-to-fine registration and pose graph-based optimization were used to build the reconstructed bodies of trucks passing through the lidar detection zone. This framework potentially could remove the occlusion and missed detection issues for a short interval of sensing duration. This framework did not contain the reconstruction to be on the ground plane. Future research is proposed to constrain the reconstruction to the road surface and, and to explore groupwise registration strategies for a potential one-stage reconstruction framework.

4. LiDAR Microscopic Trajectory Estimation and Benchmark Datasets

4.1. Introduction

The microscopic trajectory of a vehicle consists of information about its position at discrete timesteps over a defined time interval. Given such a trajectory, a vehicle's instantaneous speed, acceleration, deceleration, and other traffic state parameters can be derived(*39*). Such microscopic characteristics are necessary for better traffic operations. Microscopic trajectories are used to study and understand various traffic flow phenomena like car-following behavior, lane changing behavior, capacity drops, traffic oscillation propagation, calibrating and validating car-following models, traffic simulation models (*40–42*).These trajectories are also very important to be able to assess traffic safety by means of conforming to the speed limits, maintaining reasonable headways as well as lane positions. Surrogate safety measures (SSM) are widely used important metrics to assess traffic safety and use vehicle trajectories and interaction between vehicles to estimate SSM metrics (*43*, *44*). They are also very important input for microscopic emission models such as Comprehensive Model Emissions Model (CMEM), and Motor Vehicle Emissions Simulator (MOVES) as they consider comprehensive modeling framework for driving behavior(*45*, *46*). This chapter focuses on estimating LiDAR microscopic trajectories.

Each scan of the side-fire Lidar sensor captures all the truck bodies present in its Detection Zone (LDZ) partially. The scan will have rich information of the front portion of the truck when it is entering the LDZ, side of the truck when it is in the midsection part of the LDZ and rear portion of the vehicle when it is leaving the LDZ as shown in Figure 4.1 below.

Figure 4.1 Point Clouds representing individual scans of vehicles at various sections of LiDAR Detection Zone (LDZ)

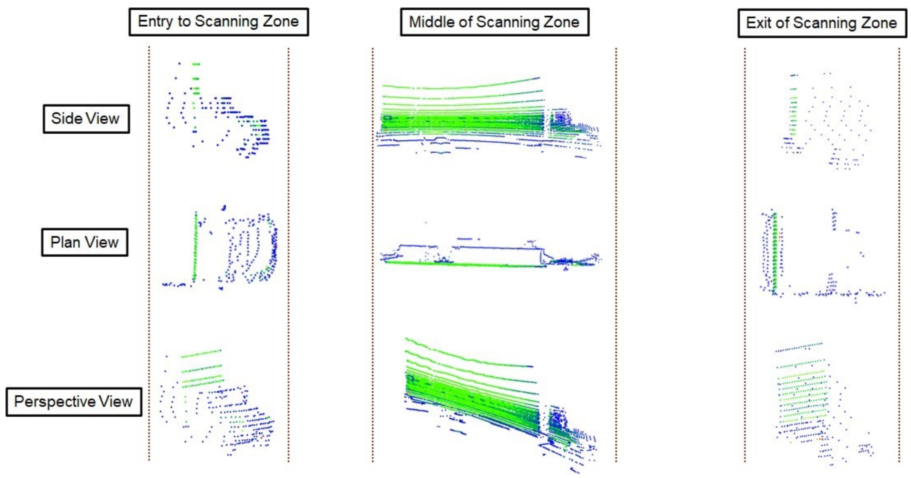

Trajectories of the vehicles passing through the LDZ can be estimated using data association and tracking of the same reference point on the corresponding raw scans of a vehicle. This reference can be a corner point of a minimum bounding box or the centroid of the bounding box either in 2D or 3D. Such an attempt was made using the centroid of a 2D bounding box of individual scans for the purpose of truck body reconstruction in (*47*). One drawback of this approach for trajectory estimation is the inherent shift in the centroid of the bounding box in successive scans ascribed to the varying size of the vehicle's point cloud as it passes through the LDZ.

When the vehicle is passing through the entry zone of the LDZ, the size (length) of the point cloud grows in each successive scan as it progressively captures more and more of the rear part of the vehicle until it reaches the mid zone of the LDZ. Due to this, the estimated centroid in each successive scan is closer to the previous centroid than it should be. Similarly, as the vehicle leaves the LDZ from midsection, each successive scan progressively loses the front portion of the vehicle. This also results in centroids in the exit zone being closer than they should be. The speed found from such trajectories would be underestimated in the entry and exit zones of the LDZ. This necessitates an alternative approach which can overcome the error due to the partial nature of the raw point clouds. To overcome these drawbacks, this research proposed a forward – backward pass rigid body transformation-based approach for estimating accurate microscopic trajectories. During the forward pass, the entire scanned body of the vehicle was reconstructed using pairwise registration. The centroid of the minimum bounding box for such reconstructed vehicle would be theoretically very close to the actual centroid of the vehicle. This fully reconstructed vehicle was projected backward to each individual scan using an inverse transformation during the backward pass. The trajectory of the vehicle was estimated using the centroid of the bounding box for these fully reconstructed vehicles. Such high temporal resolution trajectories have immense potential for further use in accurate emission estimates, traffic state estimates and traffic safety applications.

4.2. Literature Review of Related Work

4.3. Trajectory Estimation

Microscopic vehicle trajectories are critical data for understanding car-following behavior, lane changing behavior and gap acceptance which are core inputs for developing and advancing traffic flow theory, which in turn has impact on the planning, management, and operations of transport facilities. The importance of this cannot be more emphasized than by mentioning the Next Generation Simulation (NGSIM) open data (*48*, *49*). With the advances in communication and information technologies these trajectories are obtained by a variety of sensing technologies such as video-based image processing(*40–42*), global positioning systems (GPS), location based services such as cellular networks, wireless fidelity (Wi-Fi), Bluetooth based probes, license plates(*50*), and probe vehicles(*51*).

Except for video-based image techniques, all other methods provide spatially sparse trajectories known as macro trajectories. There are methods proposed to derive micro trajectories from probe vehicle based macro trajectories in the literature(*52*, *53*). Trajectories estimated from these existing Intelligent Transport System sensors have uses as well as limitations. Sometimes it takes considerable time to identify shortcomings of such data as happened in the case of the Next Generation Simulation (NGSIM) dataset collected during mid-2000s(*48*, *49*). Researchers have cautioned that without accurate empirical microscopic trajectories, "plausible but inaccurate hypotheses perpetuate in vacuum(*49*)." Also, video cameras which are only able to provide microscopic trajectories in the field of vision, have difficulty operating efficiently under all lighting conditions. LiDAR has the potential to overcome these shortcomings and to provide accurate microscopic trajectories due to its nature of providing three dimensional measurements of the target environment(*54*). LiDAR is used as a key sensor to detect and track objects in autonomous driving (*55*) and paved the way for it being tested as an infrastructure-based traffic sensing device, especially from a connected vehicles (CV) perspective to get microscopic traffic states of vehicles not equipped with CV capabilities s(*56–58*). As part of this effort researchers have proposed roadside LiDAR based microscopic trajectory estimation frameworks. Sun, Y et al. (2018) proposed a framework to extract vehicle trajectories from the 3-D LiDAR data. Their framework consists of raw data processing, statistical outlier removal of noise points, RANSAC algorithm-based ground plane segmentation to eliminate the points corresponding to the road surface, basic clustering-based algorithm to cluster points of individual vehicles, principal component analysis (PCA)-based oriented bounding box (OBB) estimation for the vehicles and a geometry-based tracking algorithm. In their study the OBB's front right corner was used for tracking the vehicle while approaching the LiDAR sensor and the rear right corner of the OBB was used while the vehicle was departing the LiDAR sensor. One of the key findings while evaluating this framework was that the estimated speed of a vehicle may suddenly drop or increase. This is attributable to the effect of using OBB of individual partial scans(*59*).

Other frameworks proposed mainly in the context of tracking road users like vehicles and pedestrians have similar steps of LiDAR raw data processing, background elimination, clustering of individual road users, classification of road users, tracking the road users using variants of Kalman Filter(*56*, *57*, *60*). All these studies track individual road users with the help of a selected reference point on their oriented bounding box like the centroid, right corner, or left corner. One thing in common for all these studies is using a bounding box of individual LiDAR scans which results in a sharp increase or decrease of the speed.

Zhang, J et al., (2019) proposed a refined tracking process using the images of LiDAR scans. In this study, a maximum distance-based background filter mask gives the moving LiDAR points of road users. Individual road users are identified using a Euclidean distance-based clustering technique. A SVM binary classifier separates vehicles from non-vehicles. They proposed an image based two-stage tracking step to overcome the bias induced due to incompleteness of individual scans. In the first stage, pairwise registration of individual LiDAR scan images is carried-out with respect to the LiDAR image of first scan to build a reference image by combining all scans. In the second stage, this reference image is invert-transformed back to each of the individual scans. The centroid of the reference image in these new positions defines the trajectory of the vehicle. One major limitation of this approach is that every LiDAR scan image should have an overlapping region with respect to the first scan image for getting accurate image registration results. This would shorten the length of an estimated vehicle trajectory. Another limitation of this approach is the warping LiDAR images would undergo during horizontal curve maneuvers which might further reduce the length of a trajectory. Another disadvantage is losing the rich third dimensional data of LiDAR sensor.

To overcome the above-mentioned shortcomings, this research proposed a forward – backward pass framework for estimating microscopic trajectories using LiDAR point clouds. The next section discusses data collection at SR-7, Calexico in Southern California. The subsequent section discusses application of the detailed steps of the proposed methodology, while the last section discusses the results and future work.

4.4. Data Collection Setup

LiDAR data was collected on State Route SR-7 (Figure 4.2) south of State Route SR-98 at Calexico, California. The data collection site had an intersection downstream of the LiDAR sensor increasing the chance of observing lane change phenomena, as shown in Figure 4.2.

Figure 4.2. LiDAR data collection site at Calexico

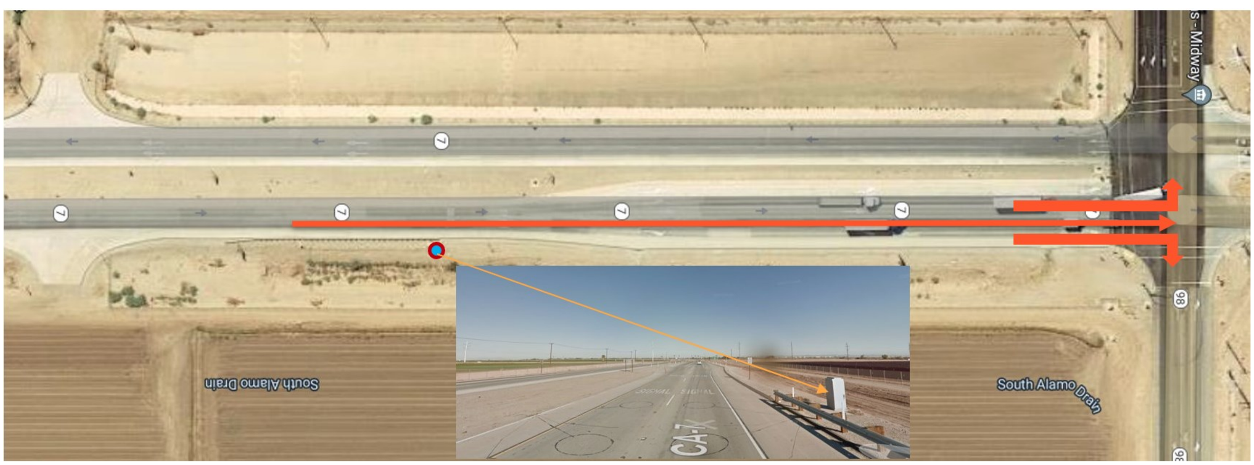

4.5. Methodology

The proposed methodology consists of processing raw LiDAR data collected through three steps. The first step involves background elimination during which all non-vehicular points are removed from the captured LiDAR data. For this purpose, a threshold-based mask filter for spatial occupancy of points was used to eliminate the background. Once the background was eliminated, the DBSCAN clustering algorithm was used for identifying all individual vehicles present in the LDZ. Once all individual vehicle points in each successive scan are collected for the duration of data collection period, it is important to group all the LiDAR scans of each single vehicle. A Global Nearest Neighbor (GNN) and Hungarian algorithm-based data association in combination with Kalman Filter-based tracking was used to establish collection of all LiDAR scans for every single vehicle that passed through the LDZ. All these three steps are explained in Li, Y et al. (*24*).

While a trajectory for the vehicle can be established during the third step mentioned earlier, it is limited in accuracy due to the following explanation. As the vehicle is passing through the LDZ, only its partial body gets scanned and is continuously varying in size. The scanned part of a vehicle body increases in size from the beginning until the mid-portion and starts decreasing after this part. This is illustrated in Figure 4.3 below. We also note that the vehicle scans at the entry and exit have a very small number of points. This induces errors in the trajectory being obtained during the tracking stage. To overcome this, a forward-backward pass approach was adopted for estimating accurate trajectories of the vehicle passing through the LDZ.

Figure 4.3. Raw LiDAR scans of vehicle while passing through LDZ

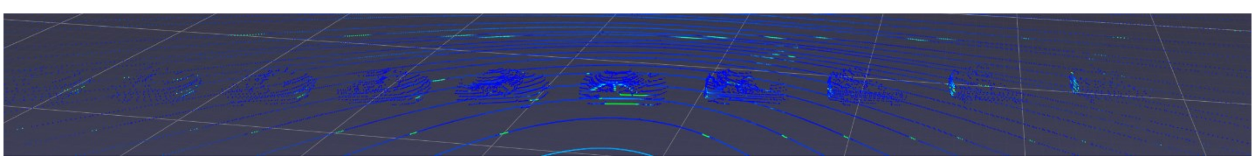

4.5.1. Identification of suitable registration pipeline for LiDAR point clouds

Identification of a robust registration pipeline combining the available registration algorithms is extremely important for the trajectory estimation purposes. The earlier registration pipeline established by Allu, et al. (*47*) does not take the road plane constraint into account. Another pipeline was established by Li, Y et al.(*61*) but excludes the LiDAR scans in the beginning and end parts of the LDZ. Hence it is necessary to determine a robust registration pipeline from the beginning to the end of the LDZ quantitatively.

4.5.2. Determination of Optimal Registration Pipeline

Identification of a robust registration pipeline with a combination of existing algorithms such that it works accurately across the entire LiDAR Detection Zone is very important. This ensures an accurate microscopic trajectory of the vehicle as well.

To identify an accurate registration pipeline, a quantitative simulation experiment was set up as follows. For every 'i^{th}' frame(scan) of the vehicle which acts as a source, a target point cloud was created by subjecting it to a known rotation of 10 degrees around the Z-axis in the road plane and a translation of 1.64 ft, 3,28 ft in X, Y-axes directions, respectively. A set of six registration pipelines has often been chosen in the literature, such as is in (*47*, *61*). These pipelines are illustrated in Figure 4.4.

Figure 4.4. Set of Registration pipelines evaluated.

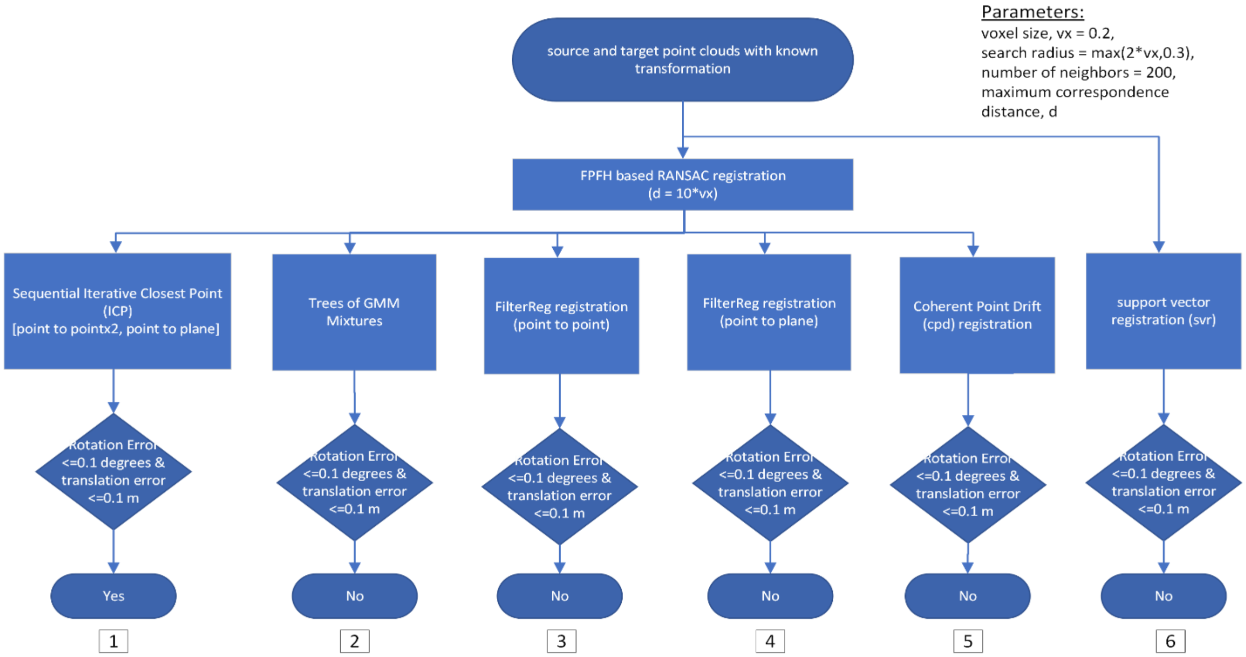

The proposed set of pipelines was tested to verify if it could estimate the 'known induced' rotation and translation accurately between each of these source and target pairs. The absolute error between induced and estimated rotations as well as translations were used to choose the appropriate registration pipeline for further use. The results of the experiment are shown in the plot presented as Figure 4.5 below.

Figure 4.5. Absolute Error between induced and estimated rotation, translations

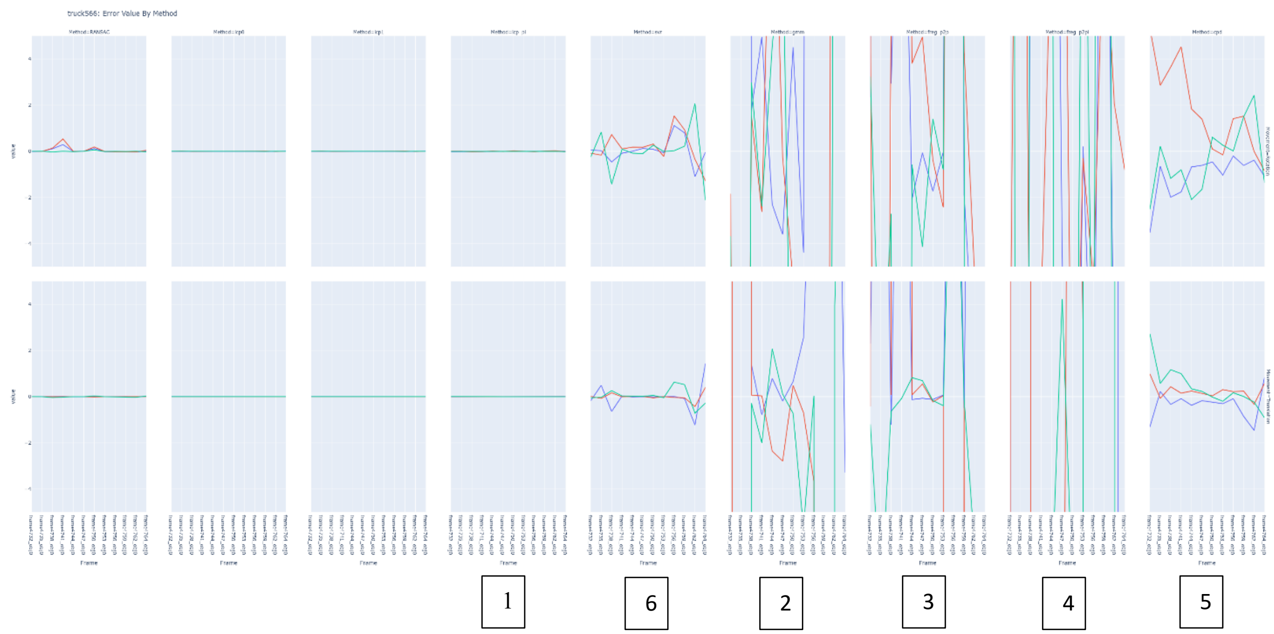

Except for the registration pipeline number 1, the other pipelines did not estimate the induced transformation accurately enough. Hence the first pipeline was used in the further steps of truck reconstruction.

4.5.3. Microscopic Trajectory Estimation

The registration pipeline chosen in the previous section is shown in Figure 4.6. This optimal pairwise registration (OPR) pipeline is used to estimate the pairwise rigid body transformation matrices between successive scans of a vehicle. For each of these transformation matrices the corresponding quality metrics fitness and RMSE values are also stored.

The fitness and RMSE values of the pairwise registration indicate its accuracy. A high fitness score and low RMSE values are desirable and from the experimental setup of registration pipelines a fitness score above 0.98 and RMSE value less than 0.2 indicates a good pairwise registration. Even though the registration pipeline is chosen based upon quantitative accuracy, the values of these metrics does not always comply to the accuracy threshold values. This can be seen in Figure 4.7 below. The example showcased is a truck which has 86 lidar scans. There are 9 discontinuities where OPR did not result in the expected accuracy. A qualitative investigation of these breakdowns can be done using Figure 4.8. showcases partial reconstructions of the truck where OPR values are continuously accurate.

Figure 4.6. Optimal Pairwise Registration Pipeline

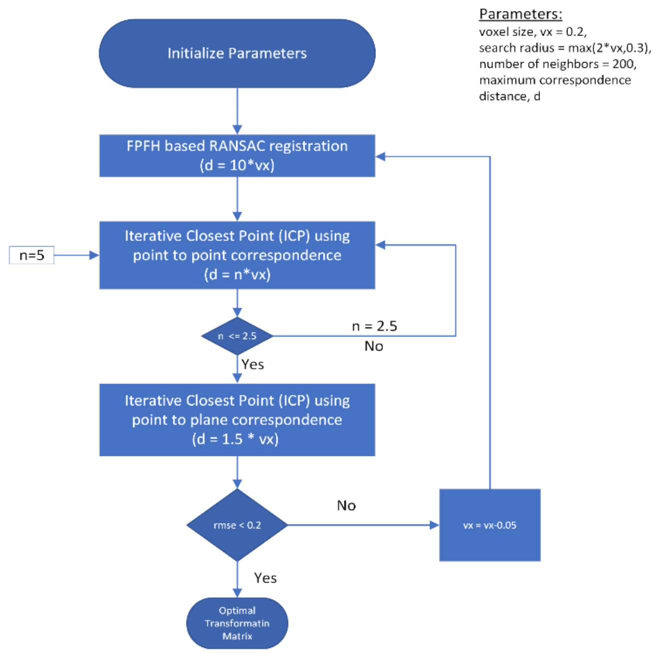

Figure 4.7. Fitness and RMSE values of OPR for a truck

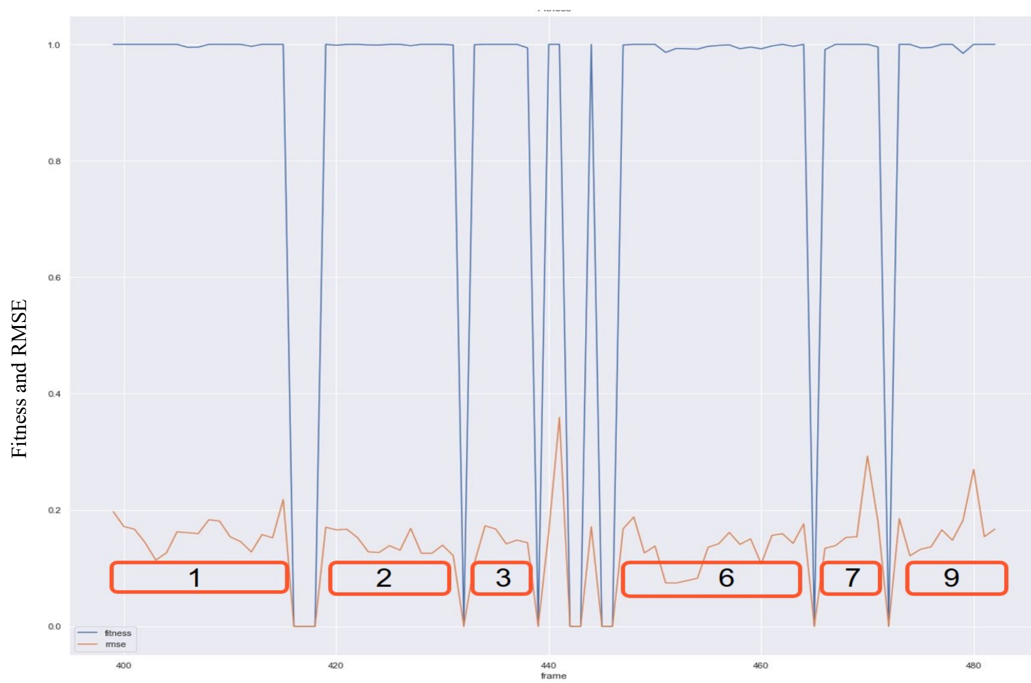

Figure 4.8. Visual Investigation of OPR breakdowns

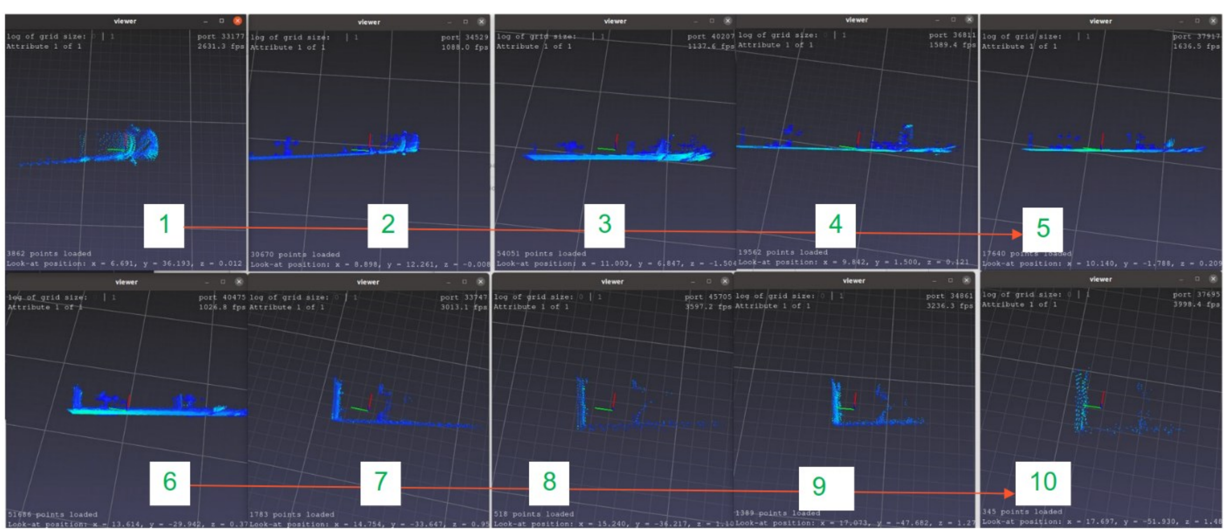

Visual investigation of the discontinuities revealed why OPR was not doing well at those discontinuities. These observations are presented in Table 4.1 below.

Table 4.1. Analysis of OPR discontinuities

Discontinuity	Explanation
Between 1 and 2	The front vertical surface of the trailer appears at greater detail compared to the scans before causing the discontinuity
Between 2 and 3	The vertical surface of trailer is not scanned as the truck is almost perpendicular to the LiDAR in this portion and lost this information compared to previous scans
Between 3 and 4	The rear vertical surface of the cab starts appearing in greater detail compared to the previous scans causing the breakdown
Between 4 and 5	The rear vertical surface s completely obscured by the side vertical face of trailer and this information is missing compared to the previous scans
Between 5 and 6	The rear vertical surface of trailer is more pronounced in 6^{th} partial reconstruction compared to the 5^{th}
Between 6 and 7	The Cab information is completely lost in 7^{th} and only half of trailer is present compared to 6^{th}
Between 7 and 8	Further breakdowns happened due to slow disappearance of the trailer's side face and rear axle.

To overcome the shortcoming of the OPR, adjacent partially reconstructed point clouds were used to obtain the transformation matrices at the discontinuities. Once all transformation matrices were obtained, the entire scanned body of the vehicle passing through the LDZ was reconstructed. The microscopic trajectory of the vehicle was obtained by performing sequential inverse rigid body transformations of the reconstructed vehicle body. The total flow of tasks involved in microscopic trajectory estimation are presented in Figure 4.9. An example trajectory of a truck passing through the LDZ is presented in Figure 4.10. A lane change captured at the beginning of the trajectory can also be observed.

Figure 4.9. Total workflow of Microscopic Trajectory Estimation

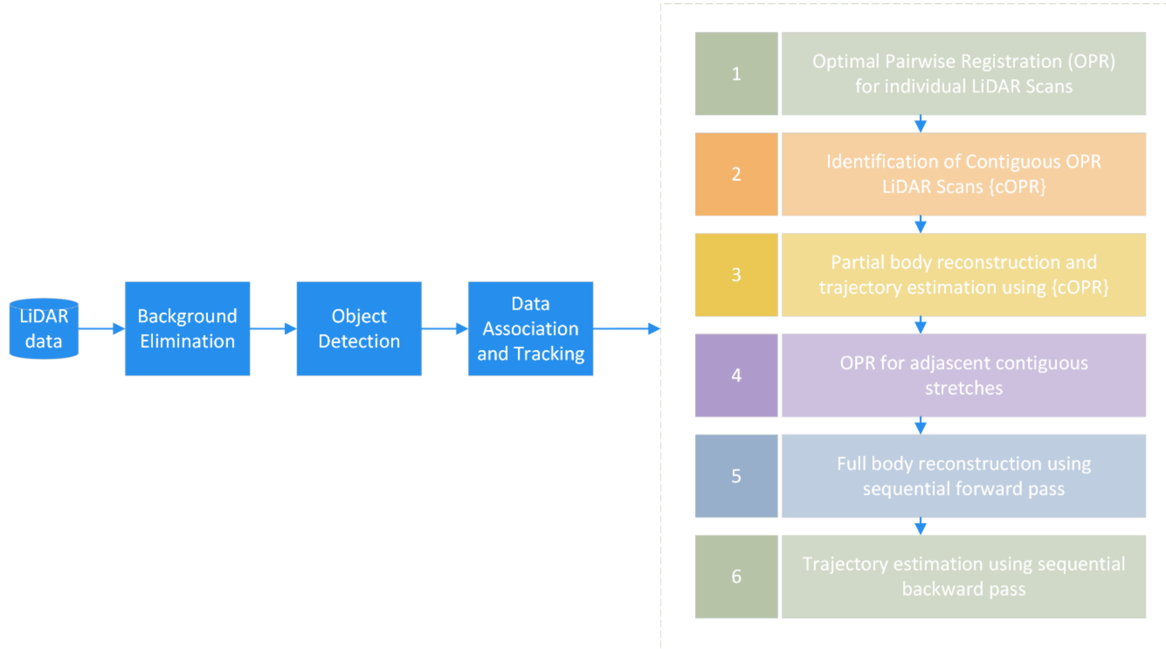

Figure 4.10. An Example Microscopic Trajectory presented at 1 Sec aggregation.

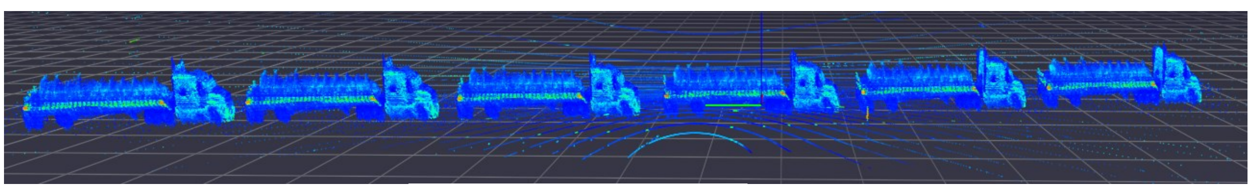

a. Side View

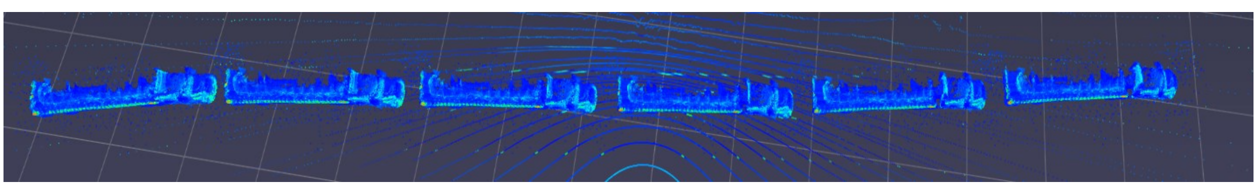

b. Top View

4.6. Analysis and Discussion

For preliminary analysis, the trajectory of the passing truck is estimated as the centroid of a 2D bounding box projected onto the road plane. Also, vehicles speed, acceleration and change in travel direction are estimated using the trajectory. A comparison of LiDAR raw scan trajectories vs reconstructed trajectories is shown in the Figure 4.11 below. With the reconstructed trajectories, the headways and lateral gaps of vehicles present in the traffic stream can be estimated.

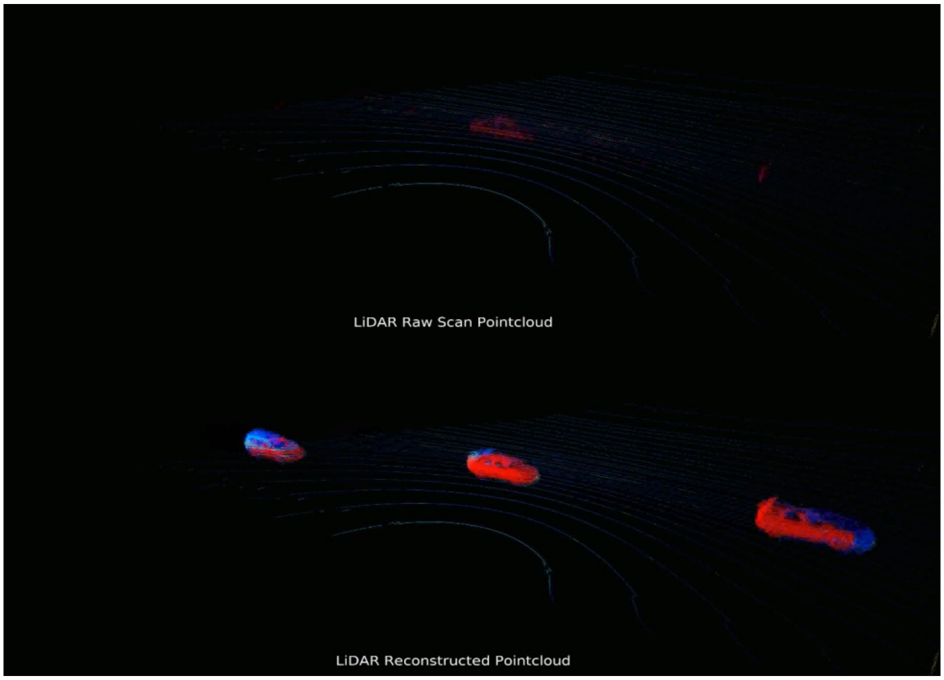

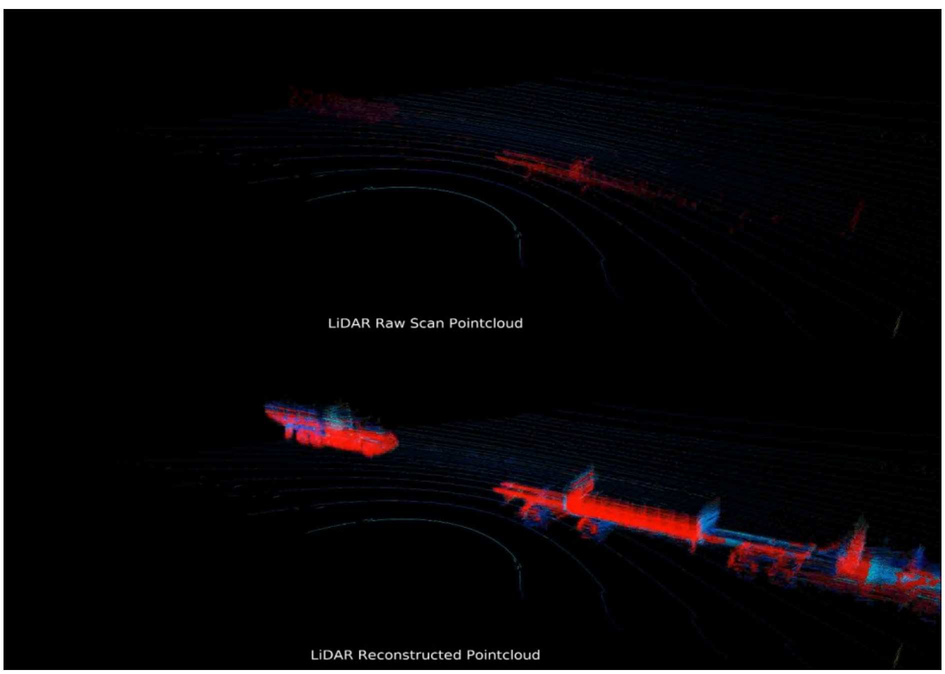

Figure 4.11. LiDAR reconstructed vs raw point clouds at Calexico

Figure 4.12. Few examples of Trajectories and corresponding traffic characteristics of the Trucks

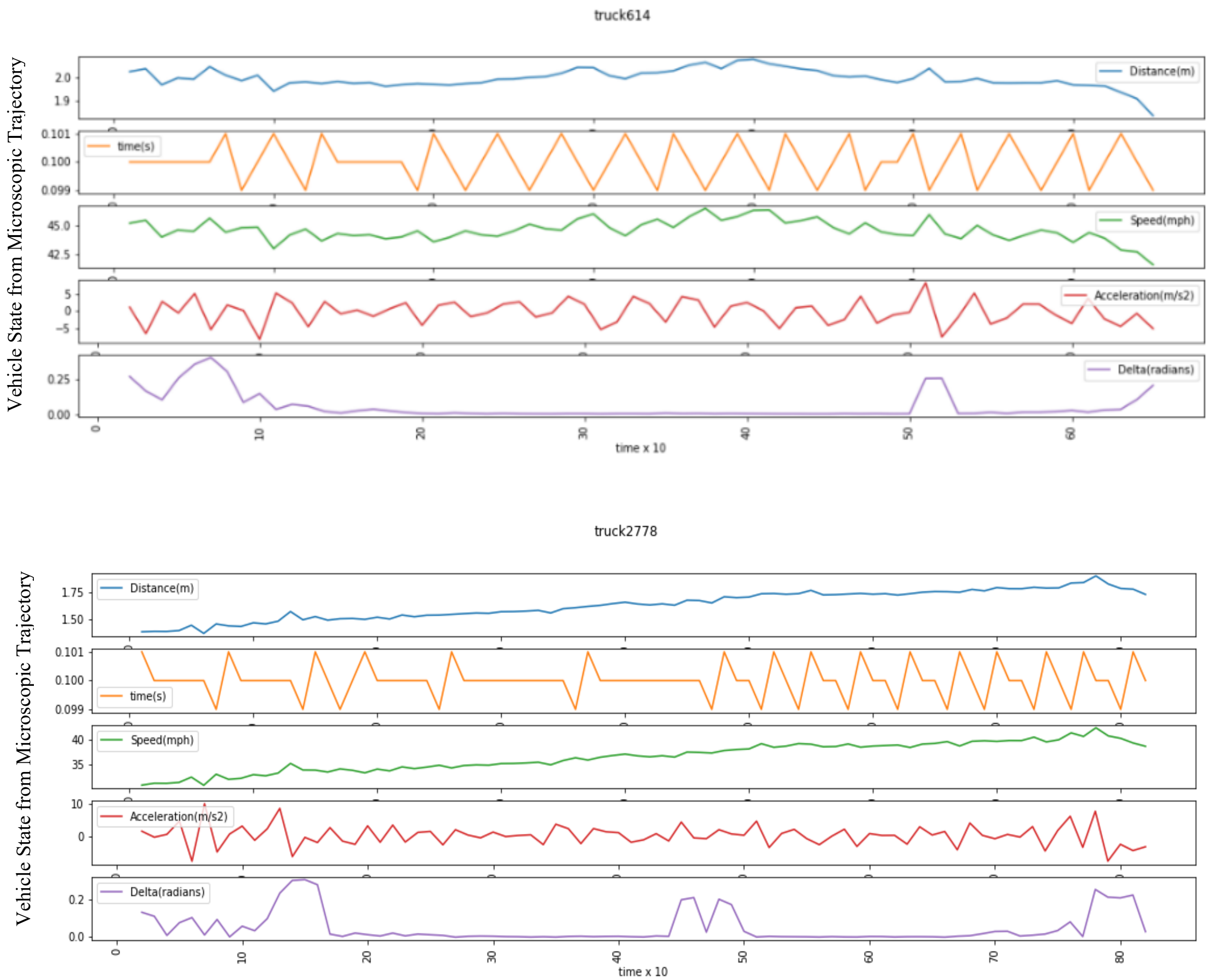

These plots show that detailed microscopic trajectories can be estimated with the proposed framework. While the trajectories appear accurate, further research is required for their validation.

5. Detection of Anomalous Microscopic Trajectories

5.1. Lateral Lane Stability of Autonomous Trucks

Autonomous heavy-duty trucks are a solution for addressing the chronic driver shortage problem the trucking industry has been facing. The increasing demand for road freight with concern for safety, fuel efficiency and the environment is creating a favorable environment for autonomous trucks(*62*). Several tech companies have ventured into developing autonomous driving technology for heavy duty trucks. Some are running pilot programs over distances greater than 200 miles(*63*).

As we move towards fully autonomous heavy-duty trucks, while at the same time cybersecurity attacks are increasing, it is valuable to have a means of assessing autonomous truck trajectories as a means of detecting and providing an alarm for anomalous behaviors. This research provides proof-of-concept that the methodologies developed here for roadside LiDAR traffic monitoring can support such an assessment.

As an illustration, the lateral positioning of truck and trailer's long edge parallel to the travel lane was estimated from the median crash barrier for a heavy-duty truck on I-710 freeway. The truck was traveling in the middle lane and triggered the LiDAR virtual loop at a time stamp of 20:00:11.919 seconds. The truck's lateral distance from the median was estimated for a duration of 2.5 seconds from the actuation of the LiDAR virtual loop. This time interval is carefully chosen as the lateral distances are computed for bounding box of individual scans. During this time interval truck is very close to the LiDAR sensor and gives consistent bounding box edges along the travel lane. The lateral offset of the closest lane marking was identified in the previous chapters.

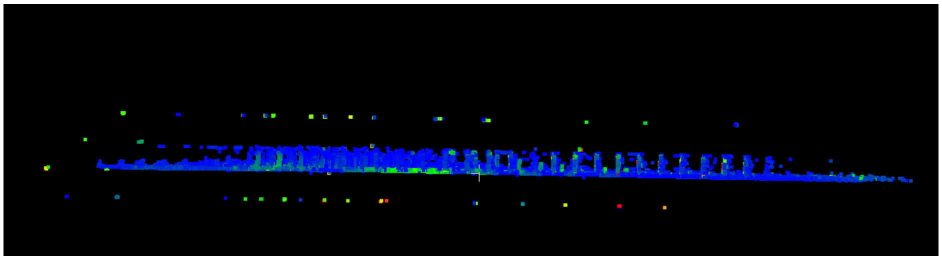

Figure 5.1. The lane positioning of a heavy duty truck

Table 5.1. Lateral offsets between Lane marking and long outer edge of the Truck

Frame Number	Median To Truck Offset(ft)	Median To Lane Offset(ft)	Lateral Offset(in)	Absolute Change in Lateral Offset (in)
104	30.34	31.72	16.56	4.56
105	29.96	31.72	21.12	0.48
106	29.92	31.72	21.6	1.44
107	30.04	31.72	20.16	1.2
108	30.14	31.72	18.96	0
109	30.14	31.72	18.96	1.68
110	30.28	31.72	17.28	0.12
111	30.27	31.72	17.4	0
112	30.27	31.72	17.4	0.84
113	30.2	31.72	18.24	0.72
114	30.26	31.72	17.52	0.96
115	30.34	31.72	16.56	0.24
116	30.36	31.72	16.32	0.96
117	30.44	31.72	15.36	0.6
118	30.49	31.72	14.76	0.72
119	30.55	31.72	14.04	9.12
120	29.79	31.72	23.16	0.24
121	29.77	31.72	23.4	0.24
122	29.75	31.72	23.64	0.84
123	29.82	31.72	22.8	1.56
124	29.95	31.72	21.24	1.44
125	29.83	31.72	22.68	2.64
126	30.05	31.72	20.04	1.08
127	30.14	31.72	18.96	0.72
128	30.08	31.72	19.68	??

The estimated lateral offset of the truck from the lane marking and the absolute change in the lateral offset as the truck was traveling through the LiDAR detection area are shown in Table 5.1. The highest value of 9.12 inches was estimated Table 5.1. Lateral offsets between Lane marking and long outer edge of the Truck between frames 119 and 120 which could be considered as indicating a significant jolt in the trajectory of the truck.

5.2. A Non-Intrusive and Influence-Agnostic Impaired Driving Detection and Control Framework using LiDAR.

Impaired driving detection is of paramount importance as it is the biggest cause of preventable traffic fatalities in the USA and has been on a rising trend in the last three years. Impaired driving also causes safety concerns for vulnerable road users, including pedestrians, pedal cyclists, and micro-mobility users, who comprise the spectrum of active mobility. Impaired driving is driving under the influence of any single or combination of alcohol, legal recreational drugs, illicit drugs, etc. To address impaired driving problems, a novel, non-intrusive, and influence-agnostic framework is proposed, consisting of a LiDAR-based microscopic trajectory estimation combined with a deep learning based impaired driving detection algorithm to flag impaired drivers; this approach is termed DUI Detection Using LiDAR (DUiDUL). Following detection, three preventative control action schemes are defined to incorporate the DUiDUL framework into the existing enforcement system.

5.2.1. Introduction

Impaired driving is associated with driving under the influence of alcohol or any of the other 400 drugs identified by NHTSA. It is one of the biggest preventable causes of traffic fatalities and was on a growing trend in the recent past(*64*). In 2020, alcohol impairment-based traffic fatalities occurred every 45 minutes and these were completely preventable as per NHTSA(*65*). A stunning

56% of drivers involved in fatal crashes tested positive for drugs(*66*). Also, a total of 38,824 traffic fatalities occurred in the United States, and a growing percentage of these fatalities, 20%, were associated with pedestrians(*67*), as is shown in Figure 1. Police patrols are not effective due to the lack of information on impaired driving activities. To address this problem, a novel framework is proposed for passively identifying and profiling erratic driving behaviors without the need for sensors embedded within the vehicle, so this strategy is "privacy-preserving" and non-intrusive.

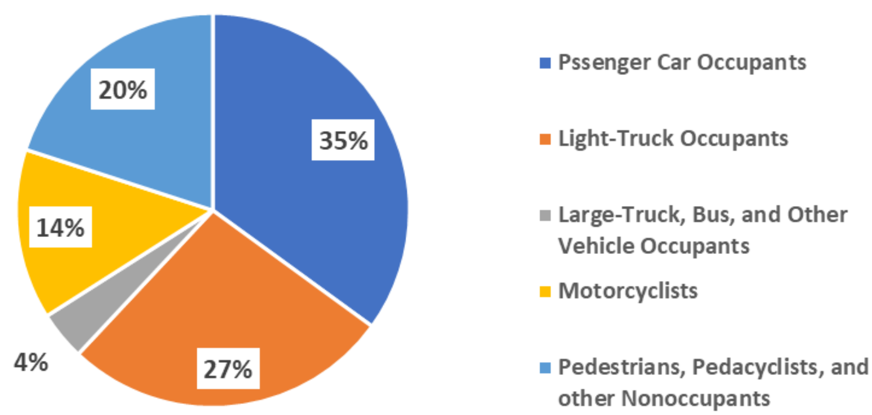

Figure 5.2. Fatality Composition by Person Type in 2020

5.2.2. LiDAR Based Impaired Driving Behavior Detection Framework

The LiDAR microscopic trajectories obtained through the advanced algorithms developed in this dissertation could also be used to identify impaired driving behavior. One such trajectory is presented in Figure 5.3 and Figure 5.4. This microscopic trajectory of the vehicle is at a temporal resolution of 0.1s.

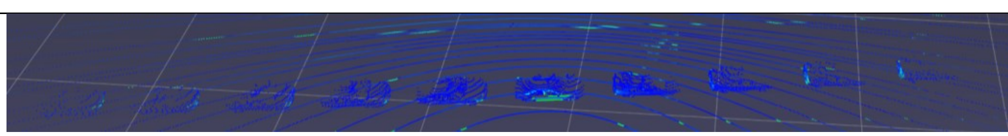

Figure 5.3. Individual LiDAR scans of a Passenger Vehicle

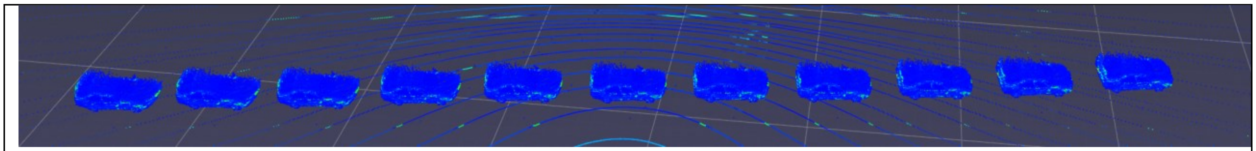

Figure 5.4. Improved dense reconstruction of passing vehicle (0.5 second granularity)

As per NHTSA, a Blood Alcohol Content (BAC) above 0.08 g/dL has observable effects on driving such as reduced ability to maintain lane position and brake appropriately, substantial impairment in vehicle control. Similar driving impairments are associated with several other drug uses as well. The high-resolution microscopic trajectories could be used as input for an appropriate feature-based deep learning pipeline to detect characteristics of impaired driving behavior and flag the vehicle. The proposed framework "DUI Detection using LiDAR" (DUiDL) is illustrated in Figure 5.5 below.

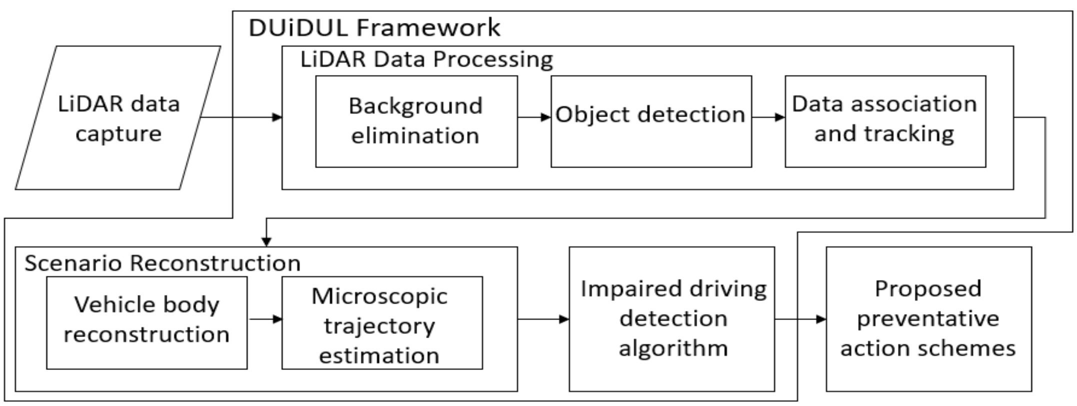

Figure 5.5. DUI Detection and Control Framework using LiDAR.

5.2.3. Other Impaired Driving Behavior Detection Devices

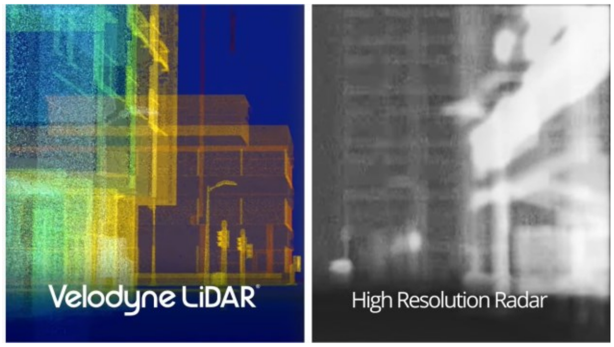

Figure 5.6. Resolution comparison of LiDAR and Radar

LiDAR can capture microscopic vehicle trajectories, including speed, acceleration, and deceleration profiles while other non-proprietary devices either cannot, or are unable to measure movements at the same resolution as LiDAR. Also, unlike currently used devices the behaviors, such as speeding, or specific influences, such as alcohol, our method can identify multiple impaired driving behaviors, and is drug influence agnostic: it can identify abnormal driving caused by all substances. The abnormal driving examples are illustrated in Figure 5.7.

Also of note, recently much effort has been made on developing methods for detecting impaired driving by directly observing the driver. There are two concerns with this approach. First, it necessitates the collection of personal information, such as a driver's face, fingerprints, or actions within the vehicle, raising serious privacy concerns. Secondly, these onboard sensing technologies may not reach a very important target demographic of young drivers aged between 16 and 29 in desired time as they disproportionately drive older vehicles(*68*, *69*). LiDAR addresses these concerns as a non-intrusive sensor.

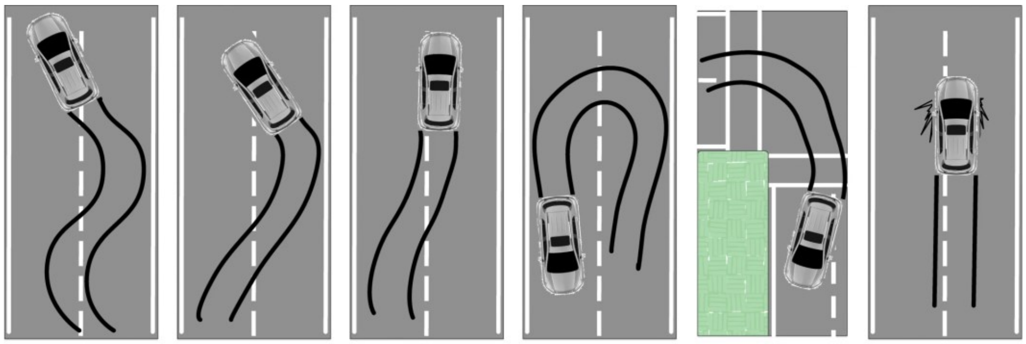

Figure 5.7. Types of abnormal driving behavior

5.2.4. Privacy-Preserving DUI Preventative Control Action Schemes

Three preventative control action schemes are proposed to incorporate DUiDUL into the existing enforcement system. They are either active, passive, or semi-active, based on whether human intervention is involved and how long the reaction time window is. The scheme is defined to be active when it accomplishes an action without any human intervention, passive when the framework supports an agency in its long-term decision (e.g. police resource allocation), and semi-active when it supports enforcement officers in short-term decision making (in near real time, e.g. pulling over a vehicle). These schemes are illustrated in Figure 5.8.

Only about 1% of drunk drivers are caught on any given day(*70*). This represents an extreme shortfall in regulation compliance and contributes to the public sentiment that one can get away with impaired driving. A semi-active control action scheme is suitable to address such sentiments, where DUiDUL is deployed to aid a field-testing police officer in the near downstream such that probable cause is established for intercepting and testing flagged drivers. This will make such testing efforts more justified and increase efficiency of testing as well.

For passive action schemes, DUiDUL assesses the percentage of drivers flagged positive for impaired driving during a given time window (e.g. 15 minutes) in the given corridor and transmits the information back to the enforcement agency's database. With sufficient deployment coverage, the agency can use this data to determine DUI hotspots for efficient and dynamic reallocation of the patrol resources. Also, trends in time of day or correlations with certain special events or holidays can be established. This will lead to better enforcement, more public compliance, and overall improved safety.

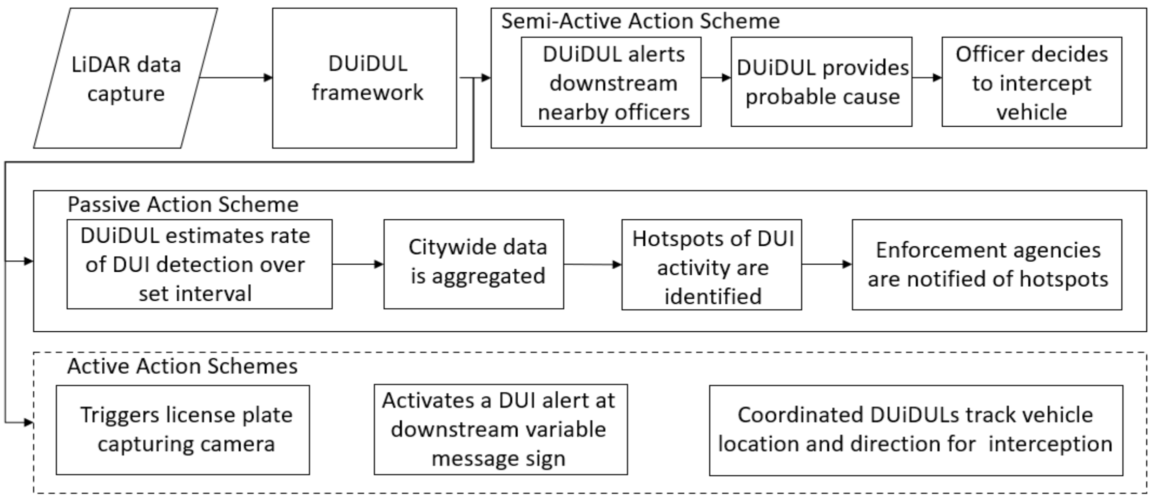

Figure 5.8. Preventative control action schemes using DUiDUL

For the active control action schemes, DUiDUL accomplishes a few possible actions either alone or in coordination with other DUiDULs without any human intervention. Some cases are explained here. The first case is where DUiDUL triggers a license plate reader for capturing the flagged vehicle's license plate for law enforcement to follow up with a DUI ticket or other suitable actions. Another case is related to warning all other nearby downstream road users about the presence of a flagged DUI driver with systems like variable message signs. An ideal case for this scheme is where multiple DUiDULs are working in a coordinated manner, where each DUiDUL can trigger a possible set of actions. An example for this is where the first DUiDUL alerts downstream road users with the help of a variable message sign and the immediate downstream DUiDUL triggers license plate capture and alerts enforcement officers to intercept the flagged driver immediately.

5.2.5. Results and Conclusion

The microscopic trajectories from Calexico are used to estimate a metric called "surrogate risk score" based on 21-dimensional descriptive statistics feature vector of speed, acceleration, and the variations in change in direction of travel. The flowchart is presented in Figure 5.9.

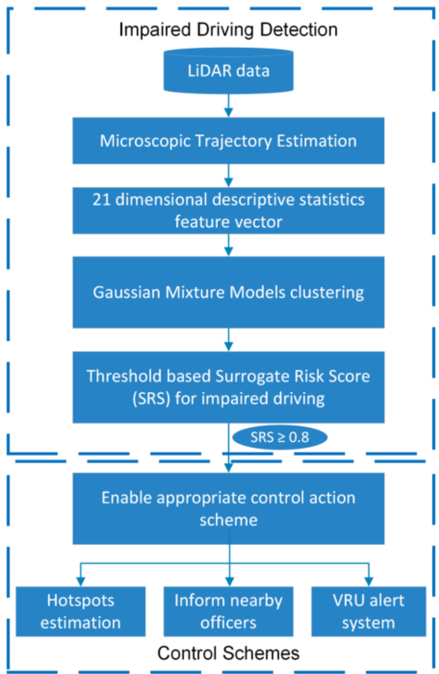

Figure 5.9. Flowchart illustrating the Impaired driving detection.

The boxplots for three features namely mean speed, standard deviation of acceleration and change in travel direction are shown in Figure 5.10

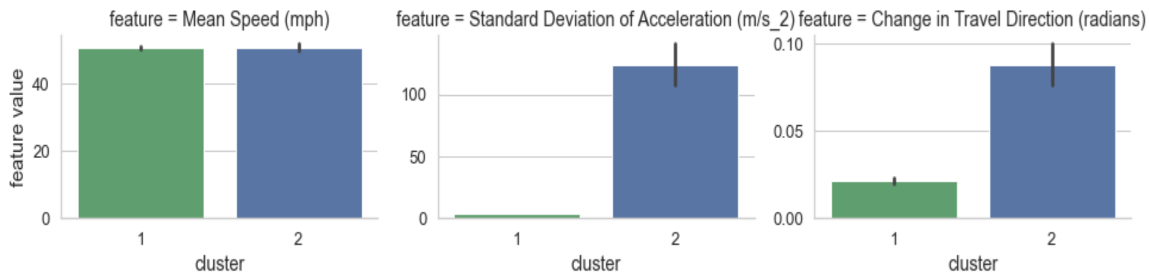

Figure 5.10. Boxplots for Mean Speed, Standard Deviation of Acceleration and Travel Direction

Of the 2,810 vehicle microscopic trajectories the Gaussian Mixture Models based clustering is used to separate into homogenous trajectories and heterogeneous trajectories. The heterogenous trajectories consist of impaired driving-based vehicles and a threshold of 80% surrogate risk score is used to estimate the impaired behavior trajectories. 1.4% of the heterogenous cluster have surrogate risk scores of more than 80%.

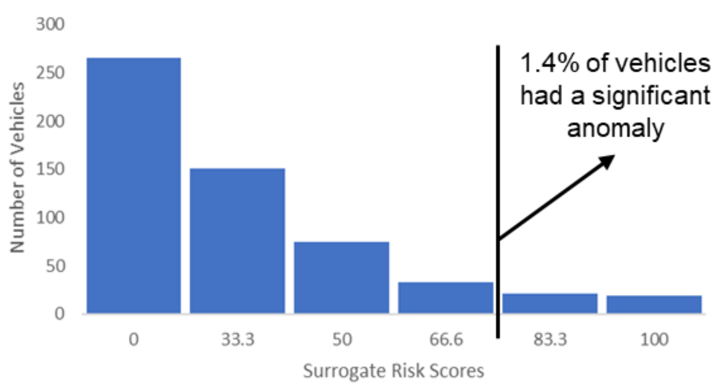

Figure 5.11. Frequency diagram of Surrogate Risk Scores

The surrogate risk score is an ad hoc measure proposed for identifying impaired driving but has scope to improve its definition and calculation procedures into the future.

6. Conclusions and Future Research

6.1. Conclusions

As part of this dissertation, infrastructure-mounted LiDAR sensors were investigated for traffic monitoring purposes, with a special emphasis on heavy-duty vehicles. The current state of practice from the literature indicates that static background subtraction for infrastructure-mounted LiDAR is done manually, selecting just the scans within the road boundaries as Regions of Interest (RoI). In the second chapter, a pipeline was proposed based on the lower bound of farthest radial distance for (i) identifying the static background, (ii) separating the road boundaries from other regions using density-based clustering, (ii) extracting lane marking using intensity values, and lane-based object detection. The proposed background algorithm applied to a dense urban freeway corridor was able to eliminate background points with high accuracy (97%). The concept of LiDAR virtual loops was then used to obtain volume counts in all three lanes of I-710 and comparisons were made with TAMS data. While the LiDAR object detection quality can be improved, instances were identified where LiDAR captured more vehicles than conventional inductive loops.

The third chapter of the dissertation presented a framework to track and group together individual scans of the same vehicle while it passed through the LiDAR Detection Zone. In the proposed framework a Hungarian Algorithm-based data association in combination with Kalman filter-based tracking was developed and used for grouping the scans corresponding to a single vehicle. While this framework provides the position of individual scans, any traffic characteristics derived from these scans will be biased as they are partial in nature. To obtain the actual dimensions of the vehicle passing through the LiDAR detection zone, a multiway registration framework was then developed and used to reconstruct the vehicle using all appropriate scans of an individual vehicle.

From this reconstructed vehicular point cloud, the actual dimensions of the vehicle like length and width were obtained.

The fourth chapter presented a forward pass-backward pass approach to estimate microscopic trajectories of the fully reconstructed vehicles. These microscopic trajectories have a temporal resolution of 0.1 seconds and all the individual vehicle state parameters such as position, speed, acceleration, deceleration could be estimated for the fully reconstructed vehicles. When the timestamps of vehicles in each of its positions are known, the interaction of individual vehicles can potentially be derived from these microscopic trajectories. These microscopic trajectories can also be used as inputs to estimate the emissions of a corridor using microscopic emission models. Further, these microscopic trajectories also have potential in determining traffic safety.

As part of chapter five, anomalous trajectories of vehicles passing through the LiDAR detection zone were identified. The developed anomaly trajectory detection acts as input in enabling a framework for anonymous impaired driving detection. Also, given the state of autonomy adaptation for heavy duty vehicles, accurate lateral positions of vehicles estimated within the lanes can be used to develop control intervention strategies in case of any failure of such autonomous trucks.

6.2. Future Work

Higher penetration rates of LiDAR sensors in vehicle detection with their ability to capture high levels of detail about the physical attributes of vehicles such as length, width, and relative position with respect to lanes and other surrounding vehicles, provides ample opportunity to develop several future applications.

The comparison study of volume counts with TAMS has shed light on possible improvement of LiDAR object detection probably with variants of Kalman Filter. Also, with the concept of virtual loops, a measure equivalent to the occupancy of Inductive Loop Detectors can be developed.

The anomalous trajectory-based applications for both impaired driving as well as safe intervention of autonomous trucks could be developed in the very near future. Also, an open-source dataset of microscopic trajectories of a LiDAR site can be developed.

Another possible extension of the current work is reidentification of the vehicles within transportation networks. The reidentification of heavy-duty trucks in particular can help in obtaining reliable travel times and estimation of origin-destination matrices, with sufficient deployment of the sensors within the network.

Also, reidentification of heavy-duty vehicles in combination with the previously developed body classification algorithms can help identify the most frequently used commodity-specific freight corridors. This would specifically be helpful for data-driven policy development in efficient deployment of emerging decarbonization technologies.

7. References

1. Tian, Y., H. Liu, and T. Furukawa. Reliable Infrastructural Urban Traffic Monitoring Via Lidar and Camera Fusion. *SAE International Journal of Passenger Cars - Electronic and Electrical Systems*, Vol. 10, No. 1, 2017. https://doi.org/10.4271/2017-01-0083.

2. Bernas, M., B. Płaczek, W. Korski, P. Loska, J. Smyła, and P. Szymała. A Survey and Comparison of Low-Cost Sensing Technologies for Road Traffic Monitoring. *Sensors (Switzerland)*, Vol. 18, No. 10, 2018. https://doi.org/10.3390/s18103243.

3. Hernandez, S. V., A. Tok, and S. G. Ritchie. Integration of Weigh-in-Motion (WIM) and Inductive Signature Data for Truck Body Classification. *Transportation Research Part C: Emerging Technologies*, Vol. 68, 2016, pp. 1–21. https://doi.org/10.1016/j.trc.2016.03.003.

4. Jeng, S.-T. (Cindy), and S. G. Ritchie. Real-Time Vehicle Classification Using Inductive Loop Signature Data. *Transportation Research Record: Journal of the Transportation Research Board*, Vol. 2086, No. 1, 2008, pp. 8–22. https://doi.org/10.3141/2086-02.

5. Tian, Y., T. Furukawa, A. Asbeck, and P. Ben-Tzvi. *Self-Powered Intelligent Traffic Monitoring Using IR Lidar and Camera*. 2016.

6. DUNN ENGINEERING ASOCIATES. *TRAFFIC CONTROL SYSTEMS HANDBOOK*. 2005.

7. Sahin, O., R. V. Nezafat, and M. Cetin. Methods for Classification of Truck Trailers Using Side-Fire Light Detection and Ranging (LiDAR) Data. *Journal of Intelligent Transportation Systems*, 2020, pp. 1–13. https://doi.org/10.1080/15472450.2020.1733999.

8. He, P., A. Wu, A. Rangarajan, and S. Ranka. *Truck Taxonomy and Classification Using*

Video and Weigh-In Motion (WIM) Technology Final Report. 2019.

9. Asborno, M. I., C. G. Burris, and S. Hernandez. Truck Body-Type Classification Using Single-Beam Lidar Sensors. *Transportation Research Record: Journal of the Transportation Research Board*, Vol. 2673, No. 1, 2019, pp. 26–40. https://doi.org/10.1177/0361198118821847.

10. Won, M. Intelligent Traffic Monitoring Systems for Vehicle Classification: A Survey. *IEEE Access*, Vol. 8, 2019, pp. 73340–73358. https://doi.org/10.1109/ACCESS.2020.2987634.

11. Bandaru, V. K. *Algorithms for LiDAR Based Traffic Tracking: Development and Demonstration Recommended Citation*. 2016.

12. Coifman, B., and H. Lee. *LIDAR Based Vehicle Classification*.

13. Vatani Nezafat, R., O. Sahin, and M. Cetin. Transfer Learning Using Deep Neural Networks for Classification of Truck Body Types Based on Side-Fire Lidar Data. *Journal of Big Data Analytics in Transportation*, Vol. 1, No. 1, 2019, pp. 71–82. https://doi.org/10.1007/s42421-019-00005-9.

14. Li, Y., A. K. Reddy, Z. Sun, A. Tok, F. G. G, and S. G. Ritchie. An Ensemble Approach to Truck Body Type Classification Using Deep Representation Learning on 3D Point Sets.

15. Lee, H., and B. Coifman. Side-Fire Lidar-Based Vehicle Classification. *Transportation Research Record: Journal of the Transportation Research Board*, Vol. 2308, No. 1, 2013, pp. 173–183. https://doi.org/10.3141/2308-19.

16. Tok, A., K. (Kate) Hyun, S. Hernandez, K. Jeong, Y. (Ethan) Sun, C. Rindt, and S. G. Ritchie. Truck Activity Monitoring System for Freight Transportation Analysis.

Transportation Research Record: Journal of the Transportation Research Board, Vol. 2610, No. 1, 2017, pp. 97–107. https://doi.org/10.3141/2610-11.

17. Bewley, A., Z. Ge, L. Ott, F. Ramos, and B. Upcroft. Simple Online and Realtime Tracking. No. 2016-Augus, 2016, pp. 3464–3468.

18. Wasser, L. A. The Basics of LiDAR - Light Detection and Ranging - Remote Sensing. *National Ecological Observatory Network*. https://www.neonscience.org/resources/learning-hub/tutorials/lidar-basics.

19. ACRONAME. THE HISTORY OF LIDAR. *https://acroname.com/*. https://acroname.com/blog/history-lidar.

20. Velodyne. Roadside Lidar Is Key to Building Smart, Safe Transportation Infrastructure. https://velodynelidar.com/blog/roadside-lidar-is-key-to-building-smart-safe-transportation-infrastructure/.

21. Zhang, Z., J. Zheng, H. Xu, and X. Wang. Vehicle Detection and Tracking in Complex Traffic Circumstances with Roadside LiDAR. *Research Article Transportation Research Record*, Vol. 2673, No. 9, 2019, pp. 62–71. https://doi.org/10.1177/0361198119844457.

22. Sun, Y., H. Xu, J. Wu, J. Zheng, and K. M. Dietrich. 3-D Data Processing to Extract Vehicle Trajectories from Roadside LiDAR Data. *Transportation Research Record: Journal of the Transportation Research Board*, Vol. 2672, No. 45, 2018, pp. 14–22. https://doi.org/10.1177/0361198118775839.

23. Wu, J. *An Automatic Procedure for Vehicle Tracking with a Roadside LiDAR Sensor Background Filtering and Lane Identification Background Filtering*.

24. Li, Y., K. R. Allu, Z. Sun, A. Y. C. Tok, G. Feng, and S. G. Ritchie. Truck Body Type Classification Using a Deep Representation Learning Ensemble on 3D Point Sets. *Transportation Research Part C: Emerging Technologies*, Vol. 133, 2021, p. 103461. https://doi.org/10.1016/J.TRC.2021.103461.

25. Derpanis, K. G. Overview of the RANSAC Algorithm. 2010.

26. Barber, C. B., and D. P. Dobkin. The Quickhull Algorithm for Convex Hulls. 1996.

27. Zhu, H., B. Guo, K. Zou, Y. Li, K. V. Yuen, L. Mihaylova, and H. Leung. A Review of Point Set Registration: From Pairwise Registration to Groupwise Registration. *Sensors (Switzerland)*, Vol. 19, No. 5, 2019, pp. 1–20. https://doi.org/10.3390/s19051191.

28. Cheng, L., S. Chen, X. Liu, H. Xu, Y. Wu, M. Li, and Y. Chen. Registration of Laser Scanning Point Clouds: A Review. *Sensors*, Vol. 18, No. 5, 2018, p. 1641. https://doi.org/10.3390/s18051641.

29. Besl, P. J., and N. D. McKay. Method for Registration of 3-D Shapes. No. 1611, P. S. Schenker, ed., 1992, pp. 586–606.

30. Pomerleau, F., F. Colas, and R. Siegwart. A Review of Point Cloud Registration Algorithms for Mobile Robotics. *Foundations and Trends in Robotics*, Vol. 4, No. 1, 2015, pp. 1–104. https://doi.org/10.1561/2300000035ï.

31. Rusinkiewicz, S., and M. Levoy. *Efficient Variants of the ICP Algorithm*.

32. Salvi, J., C. Matabosch, D. Fofi, and J. Forest. A Review of Recent Range Image Registration Methods with Accuracy Evaluation. *Image and Vision Computing*, Vol. 25, No. 5, 2007, pp. 578–596. https://doi.org/10.1016/j.imavis.2006.05.012.

33. Zhou, Q.-Y., J. Park, and V. Koltun. *Open3D: A Modern Library for 3D Data Processing*.

34. Acm Reference Format: Yilmaz, A., O. Javed, and M. Shah. Object Tracking: A Survey. *ACM Comput. Surv*, Vol. 38, 2006, p. 45. https://doi.org/10.1145/1177352.1177355.

35. Naeem, H., J. Ahmad, and M. Tayyab. Real-Time Object Detection and Tracking. *2013 16th International Multi Topic Conference, INMIC 2013*, No. December 2013, 2013, pp. 148–153. https://doi.org/10.1109/INMIC.2013.6731341.

36. Chen, X., X. Wang, and J. X. Bradley. *Tracking Multiple Moving Objects Using Unscented Kalman Filtering Techniques*.

37. Wojke, N., A. Bewley, and D. Paulus. *SIMPLE ONLINE AND REALTIME TRACKING WITH A DEEP ASSOCIATION METRIC*.

38. Choi, S., Q. Y. Zhou, and V. Koltun. Robust Reconstruction of Indoor Scenes. No. 07-12-June, 2015, pp. 5556–5565.

39. Pal, D., and M. Chunchu. Smoothing of Vehicular Trajectories under Heterogeneous Traffic Conditions to Extract Microscopic Data. *Canadian Journal of Civil Engineering*, Vol. 45, No. 6, 2018, pp. 435–445.

40. Kovvali, V. G., V. Alexiadis, and Z. Lin. Video-Based Vehicle Trajectory Data Collection. 2006.

41. Anagnostopoulos, A., and F. Kehagia. Utilizing UAVs Technology on Microscopic Traffic Naturalistic Data Acquirement. *Infrastructures*, Vol. 6, 2021, p. 89. https://doi.org/10.3390/infrastructures6060089.

42. Shi, X., D. Zhao, H. Yao, X. Li, D. K. Hale, and A. Ghiasi. Video-Based Trajectory

Extraction with Deep Learning for High-Granularity Highway Simulation (HIGH-SIM). *Communications in Transportation Research*, Vol. 1, 2021, p. 100014. https://doi.org/10.1016/J.COMMTR.2021.100014.

43. Nour, M. W. Monitoring of Microscopic Traffic Behavior for Safety Applications Using Temporal Logic. *Electronic Theses and Dissertations, 2020-*, 2021.

44. Wang, C., Y. Xie, H. Huang, and P. Liu. A Review of Surrogate Safety Measures and Their Applications in Connected and Automated Vehicles Safety Modeling. *Accident Analysis & Prevention*, Vol. 157, 2021, p. 106157. https://doi.org/10.1016/J.AAP.2021.106157.

45. Shan, X., P. Hao, X. Chen, K. Boriboonsomsin, G. Wu, and M. J. Barth. Vehicle Energy/Emissions Estimation Based on Vehicle Trajectory Reconstruction Using Sparse Mobile Sensor Data. *IEEE Transactions on Intelligent Transportation Systems*, Vol. 20, No. 2, 2019, pp. 716–726. https://doi.org/10.1109/TITS.2018.2826571.

46. Tsanakas, N., J. Ekström, and J. Olstam. Generating Virtual Vehicle Trajectories for the Estimation of Emissions and Fuel Consumption. *Transportation Research Part C: Emerging Technologies*, Vol. 138, 2022, p. 103615. https://doi.org/10.1016/J.TRC.2022.103615.

47. Allu, K. R., Z. Sun, and A. Tok. *Lidar Based Reconstruction Framework for Truck Surveillance*. 2020.

48. Next Generation Simulation (NGSIM) Open Data. https://data.transportation.gov/stories/s/Next-Generation-Simulation-NGSIM-Open-Data/i5zb-xe34. Accessed Mar. 25, 2024.

49. Coifman, B., and L. Li. A Critical Evaluation of the Next Generation Simulation (NGSIM) Vehicle Trajectory Dataset. *Transportation Research Part B: Methodological*, Vol. 105, 2017, pp. 362–377. https://doi.org/10.1016/J.TRB.2017.09.018.

50. Zhang, Z., H. Liu, L. Rai, and S. Zhang. Vehicle Trajectory Prediction Method Based on License Plate Information Obtained from Video-Imaging Detectors in Urban Road Environment. *Sensors 2020, Vol. 20, Page 1258*, Vol. 20, No. 5, 2020, p. 1258. https://doi.org/10.3390/S20051258.

51. Yao, Z., M. Liu, Y. Jiang, Y. Tang, and B. Ran. Trajectory Reconstruction for Mixed Traffic Flow with Regular, Connected, and Connected Automated Vehicles on Freeway. *IET Intelligent Transport Systems*, 2022. https://doi.org/10.1049/ITR2.12294.

52. Coifman, B., M. Wu, K. Redmill, and D. A. Thornton. Collecting Ambient Vehicle Trajectories from an Instrumented Probe Vehicle: High Quality Data for Microscopic Traffic Flow Studies. *Transportation Research Part C: Emerging Technologies*, Vol. 72, 2016, pp. 254–271. https://doi.org/10.1016/J.TRC.2016.09.001.

53. Li, Y., S. Chen, R. Du, P. Ha, J. Dong, and S. Labi Professor. Using Empirical Trajectory Data to Design Connected Autonomous Vehicle Controllers for Traffic Stabilization.

54. Barad, J. *Roadside Lidar Helping to Build Smart and Safe Transportation Infrastructure*. SAE Technical Paper, 2021.

55. Luo, Z., S. Habibi, and M. V Mohrenschildt. LiDAR Based Real Time Multiple Vehicle Detection and Tracking.

56. Chen, J., S. Tian, H. Xu, R. Yue, Y. Sun, and Y. Cui. Architecture of Vehicle Trajectories

Extraction with Roadside Lidar Serving Connected Vehicles. *IEEE Access*, Vol. 7, 2019, pp. 100406–100415. https://doi.org/10.1109/ACCESS.2019.2929795.

57. Cui, Y., H. Xu, J. Wu, Y. Sun, and J. Zhao. Automatic Vehicle Tracking with Roadside LiDAR Data for the Connected-Vehicles System. *IEEE Intelligent Systems*, 2019. https://doi.org/10.1109/MIS.2019.2918115.

58. Lv, B., H. Xu, J. Wu, Y. Tian, Y. Zhang, Y. Zheng, C. Yuan, and S. Tian. LiDAR-Enhanced Connected Infrastructures Sensing and Broadcasting High-Resolution Traffic Information Serving Smart Cities. *IEEE Access*, Vol. 7, 2019, pp. 79895–79907. https://doi.org/10.1109/ACCESS.2019.2923421.

59. Sun, Y., H. Xu, J. Wu, J. Zheng, and K. M. Dietrich. 3-D Data Processing to Extract Vehicle Trajectories from Roadside LiDAR Data. *Transportation Research Record*, Vol. 2672, No. 45, 2018, pp. 14–22. https://doi.org/10.1177/0361198118775839/ASSET/IMAGES/LARGE/10.1177_0361198118775839-FIG3.JPEG.

60. Zhao, J., H. Xu, H. Liu, J. Wu, Y. Zheng, and D. Wu. Detection and Tracking of Pedestrians and Vehicles Using Roadside LiDAR Sensors. *Transportation Research Part C: Emerging Technologies*, Vol. 100, 2019, pp. 68–87. https://doi.org/10.1016/J.TRC.2019.01.007.

61. Li, Y., Y. C. A. Tok, Z. Sun, S. G. Ritchie, and K. Allu. *Vehicle Point Cloud Reconstruction Framework for FHWA Axle-Based Classification Using Roadside LiDAR Sensor*. 2021.

62. Library of Congress. Autonomous Trucking. *The Trucking Industry: A Research Guide*. https://guides.loc.gov/trucking-industry/autonomous-trucking.

63. Clevenger, S. Autonomous Trucks Reshaping the Freight Industry. *ttnews.com*, , 2024.

64. Drugged Driving DrugFacts | National Institute on Drug Abuse (NIDA). https://nida.nih.gov/publications/drugfacts/drugged-driving. Accessed Mar. 25, 2024.

65. Drunk Driving | Statistics and Resources | NHTSA. https://www.nhtsa.gov/risky-driving/drunk-driving. Accessed Mar. 25, 2024.

66. Drug-Impaired Driving | NHTSA. https://www.nhtsa.gov/risky-driving/drug-impaired-driving. Accessed Mar. 25, 2024.

67. stewart, timothy. *Overview of Motor Vehicle Crashes in 2020*.

68. FBI — Table 33. https://ucr.fbi.gov/crime-in-the-u.s/2019/crime-in-the-u.s.-2019/topic-pages/tables/table-33. Accessed Mar. 25, 2024.

69. Teens Are the Riskiest Drivers, but They Drive the Least Safe Vehicles. https://www.iihs.org/news/detail/teens-are-the-riskiest-drivers-but-they-drive-the-least-safe-vehicles. Accessed Mar. 25, 2024.

70. Drunk Driving Archives - MADD. https://madd.org/statistic_type/drunk-driving/. Accessed Mar. 25, 2024.